Journal of Nuclear Medicine, published on November 30, 2017 as doi:10.2967/jnumed.117.200451

Evaluation of ^{11}C-Me-NB1 as a potential PET radioligand for measuring GluN2B-containing NMDA receptors, drug occupancy and receptor crosstalk

Stefanie D. Krämer[1], Thomas Betzel[1], Linjing Mu[2], Ahmed Haider[1], Adrienne Herde Müller[1], Anna K. Boninsegni[1], Claudia Keller[1], Marina Szermerski[3], Roger Schibli[1], Bernhard Wünsch[3], Simon M. Ametamey[1]

[1]Radiopharmaceutical Science, Institute of Pharmaceutical Sciences, Department of Chemistry and Applied Biosciences, ETH Zurich, CH-8093 Zurich, Switzerland

[2]Department of Nuclear Medicine, University Hospital Zurich, CH-8091 Zurich, Switzerland

[3]Institute for Pharmaceutical and Medicinal Chemistry, University of Munster, D-48149 Munster, Germany

Corresponding authors:

Prof. Simon M. Ametamey

Radiopharmaceutical Science

Institute of Pharmaceutical Sciences

ETH Zurich

Vladimir-Prelog Weg 4

CH-8093 Zurich

phone: +41 44 6337463

Simon.Ametamey@pharma.ethz.ch

Prof. Stefanie D. Krämer

Biopharmacy/Radiopharmaceutical Science

Institute of Pharmaceutical Sciences

ETH Zurich

Vladimir-Prelog Weg 4

CH-8093 Zurich

phone: +41 44 6337403

Stefanie.Kraemer@pharma.ethz.ch

Word count: 5000

Running title: PET imaging of NMDA GluN2B receptors

ABSTRACT

Clinical and preclinical research with modulators at the N-methyl-D-aspartate (NMDA) receptor GluN2B N-terminal domain (NTD) aim for the treatment of various neurological diseases. The interpretation of the results is hampered by the lack of a suitable NMDA positron-emission tomography (PET) tracer for assessing the receptor occupancy of potential drugs. We have developed ^{11}C-Me-NB1 as a PET tracer for imaging GluN1/GluN2B-containing NMDA receptors and used it to investigate in rats the dose-dependent receptor occupancy of eliprodil, a GluN2B NTD modulator. **Methods**: ^{11}C-Me-NB1 was synthesized and characterized by *in vitro* displacement binding experiments with rat brain membranes, *in vitro* autoradiography, blocking and displacement experiments by PET and PET kinetic modeling. Receptor occupancy by eliprodil was studied by PET with ^{11}C-Me-NB1. **Results**: ^{11}C-Me-NB1 was synthesized at 290±90 GBq/µmol molar activity, 7.4±1.9 GBq total activity at the end of synthesis (*n*=17) and >99% radiochemical purity. ^{11}C-Me-NB1 binding in rat brain was blocked *in vitro* and *in vivo* by the NTD modulators Ro-25-6981 and eliprodil. Half maximal receptor occupancy by eliprodil occurred at 1.5 µg/kg. At 1 mg/kg eliprodil, a dose with reported neuroprotective effects, >99.5% binding sites were occupied. *In vitro*, ^{11}C-Me-NB1 binding was independent of sigma 1 receptor (Sigma1R) and the Sigma1R agonist (+)-pentazocine did not compete for high affinity binding. *In vivo*, 2.5 mg/kg (+)-pentazocine abolished ^{11}C-Me-NB1 specific binding, indicating an indirect effect of Sigma1R on ^{11}C-Me-NB1 binding. **Conclusion**: ^{11}C-Me-NB1 is suitable for the *in vivo* imaging of NMDA GluN1/GluN2B receptors and the assessment of the receptor occupancy by NTD modulators. GluN1/GluN2B NMDA receptors are fully occupied at neuroprotective doses of eliprodil. Furthermore, ^{11}C-Me-NB1 enables imaging of GluN1/GluN2B NMDA receptor crosstalk.

Keywords: NMDA, PET, receptor occupancy, eliprodil, NTD modulator

INTRODUCTION

Pharmacological modulation of NMDA receptors may become an efficient therapeutic strategy for the treatment of cerebral ischemia, Alzheimer's, Huntington's and Parkinson's disease, depression, neuropathic pain and schizophrenia (*1*). A functional NMDA receptor consists of four subunits out of the 3 subfamilies GluN1, GluN2A-D and GluN3A,B. Typically, two subunits are GluN1 while the other two are mainly from the GluN2 subfamily (*1,2*). The receptor is co-activated by glutamate and glycine or *D*-serine. Besides the agonist binding domains, it offers additional sites for pharmacological modulation (*1,2*). Ifenprodil, eliprodil and Ro-25-6981 bind to the NTD interface of two subunits with high selectivity for GluN1/GluN2B (NTD binding site) over GluN1/GluN2A (*1,2*). Despite promising *in vitro* results with NTD modulators, effective doses in preclinical studies were often higher than expected and results from clinical trials did not hold the expectations (*3,4*). Ligand sharing between the NDT binding site and sigma receptors and the direct or indirect control of NMDA receptor activity and localization by sigma 1 receptor (Sigma1R) and dopamine receptors are among the discussed confounding factors (*5,6*).

In our efforts to develop a PET radioligand for imaging GluN1/GluN2B receptor, we developed ^{11}C-Me-NB1 (**Fig. 1**). ^{11}C-Me-NB1 is based on WMS-1405 (herein designated Me-NB1), a NTD binding site ligand derived from ifenprodil with improved metabolic stability, 5.4 nM affinity (K_i) to hGluN1/hGluN2B and no modulatory effect at hGluN1/hGluN2A receptors. It has 33- and 100-fold selectivity for hGluN1/hGluN2B over human Sigma1R and sigma 2 receptors (Sigma2R), respectively (*7*). Applying ^{11}C-Me-NB1, we characterized the distribution pattern of NTD modulator binding sites in the rat brain and investigated their dose-dependent occupancy by eliprodil (K_i=13 nM for hGluN1/hGluN2B; K_i=132 and 634 nM rat Sigma1R and Sigma2R, respectively) (*8*). Furthermore, we examined whether ^{11}C-Me-NB1 PET can be used to investigate receptor cross-talk involving GluN1/GluN2B receptors.

MATERIAL AND METHODS

Radiolabeling and i*n vitro* characterization

^{11}C-Me-NB1 was produced by reacting ^{11}C-CH_3I with 3-(4-phenylbutyl)-2,3,4,5-tetrahydro-1*H*-3-benzazepine-1,7-diol (*9*) (**Fig. 1**). The log *D* was determined by the shake-flask method with ^{11}C-Me-NB1 in n-octanol/phosphate-buffered saline pH 7.4. Binding affinities were determined in competition binding assays with rat brain membranes (*10*-*12*). For autoradiography, horizontal rat brain slices of adult male Wistar rats or Sigma1R knockout mice, lacking the Sigma1R encoding genomic sequence with the exception of the first four codons (*13*) and wild type mice were incubated with ^{11}C-Me-NB1 alone or in combination as indicated.

Ex vivo biodistribution

Animal experiments were in accordance with the Swiss legislation on animal welfare and approved by the Veterinary Office of the Canton Zurich, Switzerland. Twelve male Wistar rats (296-373 g) were injected awake into a tail vein (i.v.) with 2 mL/kg eliprodil vehicle (5 % glucose, 0.45 % NaCl, 1 mM citric acid pH 7) or 2 mg/kg eliprodil (1 mg/mL) and 1 min later with 3.1-36.3 MBq (0.5-1.6 nmol/kg) ^{11}C-Me-NB1 in 250 µL saline containing ≤8% ethanol. Rats were sacrificed by decapitation under isoflurane anesthesia 15 min after tracer injection. Tissues were dissected, weighed, radioactivity was quantified and standardized uptake values (SUV, **Supplemental Fig. 1**) were calculated.

PET experiments with an input function

Seven male Wistar rats (331-353 g) were scanned with simultaneous recording of the blood coincidences (*14*). In brief, anesthesia was initiated with 5% isoflurane 40-60 min before scan start and maintained at 2.5-5% isoflurane. An arterio-venous shunt was applied by cannulation of the tail artery and a lateral tail vein. The rat was transferred to the scanner bed (Super Argus PET/CT scanner, Sedecal,

Madrid, Sprain; axial field of view 4.8 cm; spatial resolution 1.6-1.7 mm (full width at half maximum) (*15*)) and the shunt was guided through a twilite coincidence counter (swisstrace, Zurich, Switzerland) and a peristaltic pump (200-300 µL/min). The blood counter and PET scanner were started and at time zero, 32-52 MBq (0.44-0.78 nmol/kg, 250-300 µL) ^{11}C-Me-NB1 were injected via a separate, cannulated tail vein. Data were acquired for 60 min, followed by a CT. Rats were euthanized under anesthesia immediately after the scan. Between 28 and 31 min before scan start, rats were injected intraperitoneally with either 25 mg/kg ketamine in water (25 mg/mL; 3 rats) or water alone (1 mL/kg; 4 rats). Two (with ketamine) and 3 (baseline) blood curves were available for analysis, as the arterio-venous shunt became clogged in 2 rats. The ratios of parent tracer/total radioactivity in plasma and homogenized brain were determined from additional rats. The radioactivity ratio plasma/whole blood was 1.11.

PET experiments without an input function

Twenty-three Wistar rats (327-409 g) were scanned as described above, without an arterio-venous shunt. Anaesthesia was induced 15-35 min before tracer injection. Test compounds in <1mL vehicle (Me-NB1 same as eliprodil; (+)-pentazocine, 0.1 M HCl/Ringer lactate, 2:8; Ro-25-6981, 1:1 polyethylene glycol 300/saline) were injected i.v. on the scanner bed under anesthesia 1 min (Me-NB1, eliprodil, (+)-pentazocine), 5 min (Ro-25-6981) or 20 min (haloperidol, (*16*)) before ^{11}C-Me-NB1. Injected doses of ^{11}C-Me-NB1 were 20-89 MBq, total doses of ^{11}C-Me-NB1 and Me-NB1 were 0.4-3000 nmol/kg (0.00013-1 mg/kg), eliprodil 0.7-5700 nmol/kg (0.00025–2 mg/kg), Ro-25-6981 16.4 µmol/kg (7.5 mg/kg, free base), haloperidol 346 nmol/kg (0.13 mg/kg; Haldol, Janssen-Cilag, Schaffhausen, Switzerland) and (+)-pentazocine 8.8 µmol/kg (2.5 mg/kg). For baseline scans, the respective vehicle was injected. In a displacement experiment, 1 mg/kg eliprodil in 450 µL vehicle was injected into a tail vein 20 min after scan start.

PET data reconstruction and analysis

PET data were reconstructed as described in **Supplemental Fig. 1**. Images and time-activity curves (TAC) were generated with PMOD v3.7 (PMOD Technologies, Zurich, Switzerland) with predefined regions of interest, modified from the PMOD template (**Supplemental Fig. 1**). Scans with an input function were analyzed with Matlab (MathWorks, Natick, MA) by compartment modelling (*14,17*). In brief, the clearance parameter of tracer transfer from plasma to brain (K_1), the rate constants of transfer out of the brain (k_2), receptor binding (k_3) and dissociation from the receptor (k_4), as well as the K_1 and k_2 of the radiometabolite (K_{1M}, k_{2M}) were fitted for whole brain for the full scan duration, and the respective volume of distribution (V) of total tracer ($V_{T,fit}=K_1/k_2\times(1+k_3/k_4)$), V of specifically bound tracer ($V_S=K_1/k_2\times k_3/k_4$), V of non-displaceable tracer ($V_{ND}=K_1/k_2$) and the V ratio V_T/V_{ND} (DVR) and binding potential ($BP_{ND}=k_3/k_4$=DVR-1) were calculated (*17,18*). V_T was in addition determined from the Logan plot ($V_{T,Logan}$), (*17,19*). Blood coincidence start time and background, and a bi-exponential function describing the ratio parent/total radioactivity in plasma were fitted together with the rate constants. Results were confirmed with the PKIN module of PMOD v3.9. For the fits of the individual brain regions and truncated scan durations, only K_1 to k_4 were fitted, all other parameters were used as fitted for whole brain.

For quantification without an input function, SUV was averaged from 0 to 60 min ($SUV_{0\text{-}60min}$). For the receptor occupancy study, $SUV_{0\text{-}60min}$ were fitted with the function in Equation 1.

$$SUV_{0\text{-}60min}=(SUV_{0\text{-}60min,max} - SUV_{0\text{-}60min,min}) \times D_{50}/(D_{50}+d) + SUV_{0\text{-}60min,min} \quad \text{Eq. 1}$$

$SUV_{0\text{-}60min,min}$ and $SUV_{0\text{-}60min,max}$ are the plateaux, d is the sum of the eliprodil and ^{11}C-Me-NB1/Me-NB1 doses, with the latter multiplied with a weighting factor f. The fitted parameters were D_{50}, f, $SUV_{0\text{-}60min,min}$ and $SUV_{0\text{-}60min,max}$. Receptor occupancy ($d/(D_{50}+d)$) was calculated by re-arranging Equation 1. Specific binding in % was calculated as $(SUV_{0\text{-}60min,max}\text{-}SUV_{0\text{-}60min,min})/SUV_{0\text{-}60min,max}*100\%$.

Statistical analysis

Mean values are shown with standard deviations and compared by a homoscedastic, 2-tailed Student's t-test (without correction for multiple comparisons). The Akaike information criterion, corrected for finite sample size was calculated according to (*20*).

RESULTS

Tracer radiosynthesis and *in vitro* characterization

Radiolabeling with carbon-11 was accomplished by reacting the phenolic precursor with ^{11}C-MeI to afford ^{11}C-Me-NB1 (**Fig. 1**) in 290±90 GBq/μmol molar activity and 7.4±1.9 GBq total activity at end of synthesis (*n*=17). Radiochemical purity was >99%. Total synthesis time from end of bombardment was 35-40 min. Log *D* at pH 7.4 was 1.4±0.2 (*n*=3). In the *in vitro* competition binding assay, Ro-25-6981 (7.2 nM affinity to the human NTD binding site, similar affinity to guinea pig Sigma1R and Sigma2R (*21,22*)) competed with the binding of both ^{3}H-ifenprodil and the SigmaR1 agonist (+)-^{3}H-pentazocine with two-digit nanomolar K_i (see **Supplemental Table 1** for details). Haloperidol, an antagonist for D2, D3 and D4 receptors and inverse agonist of Sigma1R (*7,23*), competed in the micromolar range with ^{3}H-ifenprodil (20 and 37°C) and (+)-^{3}H-pentazocine (20°C) but with two-digit nanomolar K_i with (+)-^{3}H-pentazocine at 37°C. The K_i for the competition of eliprodil with ^{3}H-ifenprodil was 48.5±32.0 nM (20°C), in agreement with previous findings (*4*). Its competition with (+)-^{3}H-pentazocine was weak (K_i ≥229 nM, 37°C). Me-NB1 bound with K_i 40.2±2.8 nM in competition with ^{3}H-ifenprodil but only weakly competed with (+)-^{3}H-pentazocine (IC_{50} >4 μM, 37°C), confirming a high selectivity of Me-NB1 for the rat NTD binding site over rat Sigma1R.

^{11}C-Me-NB1 autoradiography and biodistribution

In vitro autoradiography revealed binding of ^{11}C-Me-NB1 throughout the brain. Binding was reduced by eliprodil (54 nM, 10 μM), Ro-25-6981 (100 μM), haloperidol (10 μM) or an excess of Me-NB1 (100 μM) but not by 1 mM glutamate (**Supplemental Fig. 2**). Specific binding was confirmed in *ex vivo* biodistribution experiments (**Supplemental Fig. 3**)**.** Brain SUV values were 3.8±1.2 for midbrain, 3.7±1.0 for cortex, 2.8±0.8 for cerebellum and 2.7±0.7 for olfactory bulb (*n*=8). Eliprodil (2 mg/kg i.v.) reduced ^{11}C-Me-NB1 accumulation in all brain regions. The relative reduction was highest for midbrain, brain

stem, cortex and striatum (all >40% and significant) and lowest and not significant for hippocampus (31.9%) and cerebellum (34.5%). In peripheral tissues, accumulation was highest in adrenal glands (SUV 10.3±2.9, 52.9% specific). The SUV in blood was significantly (p=0.002) higher under blocking (0.300±0.035) than baseline (0.194±0.045) conditions.

^{11}C-Me-NB1 PET and PET kinetic modelling

Fig. 2 shows PET images under baseline and blocking conditions. TACs of ^{11}C-Me-NB1 in various brain regions and after blocking and displacement with eliprodil are shown in **Fig. 2** and **Supplemental Fig. 4**. Both blocking and displacement reduced the SUV, further confirming the specific and reversible binding of ^{11}C-Me-NB1.

Data of 5 scans with an arterial blood TAC were available, and brain TACs were fitted to a one- and two-tissue compartment model. The presence of a polar radiometabolite in plasma and up to 7% in brain (determined from brain homogenates) were taken into account for the analysis (**Fig. 3**). Fits with a two-tissue compartment model and the respective Logan plots are shown in **Fig. 3** (whole brain) and **Supplemental Figs. 5 and 6** (regions). Parametric maps for V_T for the scan in **Fig. 2A** are shown in **Supplemental Fig. 7**. $V_{T,fit}$ and $V_{T,Logan,}$ of 12 brain regions each of the 5 scans are depicted in **Supplemental Fig. 8**. **Supplemental Fig. 9** shows the fit of the data in **Fig. 3** with a one-tissue compartment model and the residuals for both models. The Akaike information criterion favored the two-tissue compartment model. For all scans, $V_{T,fit}$ of whole brain remained within ±5% when the scan end time for data analysis was reduced to any time between 13 and 60 min (**Fig. 3D**). Ignoring radiometabolite distribution to the brain resulted in similar fit parameters. **Supplemental Tables 2 to 4** show the fit parameters for whole brain of the individual scans. Averaged for the five scans and for whole brain, $V_{T,fit}$ was 11.8±0.7, BP_{ND} 3.77±0.97 and V_{ND} 2.57±0.56. Average K_1 was 2.9±0.9 mL/cm^3/min, k_2 1.2±0.6 min^{-1}, k_3 0.73±0.09 min^{-1} and k_4 0.20±0.04 min^{-1}.

PET quantification without an arterial input function and effect of ketamine

As a reference region without specific binding of ^{11}C-Me-NB1 was not available for input-function independent analysis (*17*), $SUV_{0\text{-}60\ min}$ was evaluated as a surrogate for V_T. Pearson's r^2 for the linear correlation between $SUV_{0\text{-}60min}$ and $V_{T,fit}$ of 5 rats (12 brain regions) was 0.913 (**Supplemental Fig. 8B**). The transformed (according to the correlation) $SUV_{0\text{-}60min}$ of all 4 baseline scans and 3 scans after ketamine challenge were in agreement with $V_{T,fit}$ values (**Supplemental Fig. 10**). The sub-therapeutic dose of ketamine was administered to investigate whether changes in glutamate levels affect ^{11}C-Me-NB1 accumulation (*24*). Our results (V_T and $SUV_{0\text{-}60min}$) excluded a major influence of ketamine on ^{11}C-Me-NB1 accumulation under isoflurane anesthesia (**Supplemental Fig. 10**, **Supplemental Tables 3, 4**).

Receptor occupancy by eliprodil

Using ^{11}C-Me-NB1, we determined the dose-dependent occupancy of the NTD binding sites by eliprodil. D_{50} was 4.2 nmol/kg (1.5 µg/kg) for whole brain (**Fig. 4**). The fit dose to reach 99% occupancy was 150 µg/kg. Specific binding was 46.9%. Fits for individual brain regions revealed D_{50} values between 3.2 and 7.3 nmol/kg (**Supplemental Fig. 11**). Non-displaceable tracer uptake had no effect on D_{50} (**Supplemental Fig. 12**). A Lassen plot analysis (*25*) revealed D_{50}=8.5 nmol/kg (**Supplemental Fig. 13**).

Imaging receptor crosstalk with ^{11}C-Me-NB1

NMDA receptor activity is modulated by Sigma1R and dopamine receptors (*6,26,27*). We used (+)-pentazocine and haloperidol to modulate Sigma1R and dopamine receptors, respectively. Both (+)-pentazocine and haloperidol showed only weak competition with ^{3}H-ifenprodil in the competition binding assays. (+)-Pentazocine brain concentrations were aimed at 350-2000 nM (*28*) and the dose of haloperidol corresponded to 10-fold the D_{50} in a D2/D3 receptor occupancy study with ^{11}C-raclopride in rats (*16*). At these concentrations, Sigma1Rs and D2/D3 receptors, respectively, should be occupied,

while no direct binding to GluN1/GluN2B receptors should occur. Both haloperidol and (+)-pentazocine abolished ^{11}C-Me-NB1 specific binding under these conditions (**Fig. 5A**).

To definitely exclude both a direct competition between ^{11}C-Me-NB1 and (+)-pentazocine binding and high affinity binding of ^{11}C-Me-NB1 to Sigma1R, we performed *in vitro* autoradiography with brain slices from Sigma1R knockout mice (**Fig. 5E,F, Supplemental Fig. 14**). ^{11}C-Me-NB1 binding was not different between slices from wild type and Sigma1R knock out mice, excluding significant binding of ^{11}C-Me-NB1 to Sigma1R. (+)-Pentazocine (1 µM) reduced the binding for both genotypes by < 10% ($p < 0.05$) while the same concentration of eliprodil reduced the binding for both genotypes by 40% ($p < 0.01$), similar as in the *ex vivo* biodistribution experiment and receptor occupancy study. Autoradiography at 3 different ^{11}C-Me-NB1 concentrations revealed high-affinity binding in all brain regions of rat, mouse and Sigma1R knockout mouse, including the GluN2B-free cerebellum, in agreement with the PET results.

DISCUSSION

Till to date, no clinically validated PET radioligand exists for the imaging of NMDA receptors. Reasons for failure include lack of *in vivo* specificity and selectivity, low affinity, poor metabolic stability and poor distribution to the brain (*29-34*). Aiming to overcome the shortcomings of previously reported radioligands and given the excellent *in vitro* properties of Me-NB1 we developed ^{11}C-Me-NB1 for imaging GluN2B receptors. ^{11}C-Me-NB1 was obtained in high radiochemical yields and molar activities. *In vivo*, it followed a two-tissue compartment model, with $SUV_{0\text{-}60min}$ as a useful surrogate for V_T, but *cave* its inherent high variability (*17*).

^{11}C-Me-NB1 binding was competed by low doses of eliprodil in all brain regions, including midbrain, pons and cerebellum with low GluN2B levels (*35-38*). Off-target binding to Sigma1R was excluded *in vitro*. The GluN2B-poor regions contain significant levels of GluN2D or GluN2C (*36*). ^{11}C-Me-NB1 and eliprodil may bind to these or alternative GluN receptor subtypes in addition to GluN1/GluN2B receptors. The high specific binding of ^{11}C-Me-NB1 in adrenal glands, a tissue containing GluN1, GluN2C and GluN2D but not GluN2A or GluN2B (*39*) supports this hypothesis.

In preclinical studies, eliprodil had neuroprotective effects at 1 mg/kg (*4,40,41*). This corresponds to full (≥99.5%) receptor occupancy in our study. As discussed by Carter *et al.* (*4*), antidepressant and anticonvulsive effects observed at even higher doses may have resulted from lower-affinity binding to alternative targets.

The Sigma1R agonist (+)-pentazocine abolished ^{11}C-Me-NB1 specific binding in the rat brain despite the lack of direct competition *in vitro*. (+)-Pentazocine stabilizes the Sigma1R in its dimeric/monomeric form(s), which interacts with other proteins (*23*). Besides indirect effects on NMDA receptors, *e.g.*, phosphorylation, a direct interaction between Sigma1R and the N-terminal domain of GluN1 that is involved in the interface with the GluN2B NTD was recently demonstrated (*42*). This

interaction may directly hamper ^{11}C-Me-NB1 binding. Alternatively, direct and/or indirect NMDA receptor modulation could bring the receptor to a conformation with reduced binding affinity for NTD ligands. Finally, altered receptor trafficking and cell-surface density could affect ^{11}C-Me-NB1 accumulation.

Several mechanisms could result in the elimination of ^{11}C-Me-NB1 specific binding observed with haloperidol. Activation of dopamine receptors modulates NMDA receptor-mediated Ca^{2+} currents and treatment of rats with 1 mg/kg haloperidol altered the phosphorylation pattern of GluN1 and GluN2B (*6,26,43,44*). Haloperidol furthermore modulates sigma receptors (*7,45*). We did not further investigate on the molecular mechanisms. However, our data suggest that ^{11}C-Me-NB1 PET could become a useful tool to visualize the consequences of receptor crosstalk involving GluN2B-containing NMDA receptors.

CONCLUSION

We have successfully developed ^{11}C-Me-NB1 that allows to non-invasively image the density of NTD binding-site containing NMDA receptors. This may allow in the future to follow non-invasively the density of GluN2B/GluN1A receptors in neuronal diseases and to study the receptor occupancy under therapeutic intervention. Our receptor-occupancy study suggests that published neuroprotective effects of eliprodil in rats required complete occupancy of the NTD binding sites. ^{11}C-Me-NB1 PET is sensitive to drug-induced receptor crosstalk.

FUNDING AND DISCLOSURE

This work was financially supported by the Swiss National Science Foundation (SNSF, Grant Nr. 160403).

ACKNOWLEDGMENTS

We thank Bruno Mancosu for tracer production and Jose Miguel Vela Hernandez for providing us with Sigma1R$^{-/-}$ and wild-type mouse brain tissues.

REFERENCES

1. Paoletti P, Bellone C, Zhou Q. NMDA receptor subunit diversity: impact on receptor properties, synaptic plasticity and disease. *Nat Rev Neurosci.* 2013;14:383-400.

2. Monaghan DT, Irvine MW, Costa BM, Fang G, Jane DE. Pharmacological modulation of NMDA receptor activity and the advent of negative and positive allosteric modulators. *Neurochem Int.* 2012;61:581-592.

3. Ikonomidou C, Turski L. Why did NMDA receptor antagonists fail clinical trials for stroke and traumatic brain injury? *Lancet Neurol.* 2002;1:383-386.

4. Carter C, Avenet P, Benavides J, et al. Ifenprodil and Eliprodil: Neuroprotective NMDA Receptor Antagonists and Calcium Channel Blockers. In: Herrling PL, ed. *Excitatory Amino Acids: Clinical Results with Antagonists*. Waltham (MA): Academic Press - Elsevier; 1997.

5. Nguyen L, Lucke-Wold BP, Mookerjee SA, et al. Role of sigma-1 receptors in neurodegenerative diseases. *J Pharmacol Sci.* 2015;127:17-29.

6. Wang M, Wong AH, Liu F. Interactions between NMDA and dopamine receptors: a potential therapeutic target. *Brain Res.* 2012;1476:154-163.

7. Tewes B, Frehland B, Schepmann D, Schmidtke KU, Winckler T, Wunsch B. Design, synthesis, and biological evaluation of 3-benzazepin-1-ols as NR2B-selective NMDA receptor antagonists. *ChemMedChem.* 2010;5:687-695.

8. Hashimoto K, London ED. Interactions of erythro-ifenprodil, threo-ifenprodil, erythro-iodoifenprodil, and eliprodil with subtypes of sigma receptors. *Eur J Pharmacol.* 1995;273:307-310.

9. Larsen P, Ulin J, Dahlstrom K, Jensen M. Synthesis of [11C]iodomethane by iodination of [11C]methane. *Appl Radiat Isot.* 1997;48:153-303.

10. Milicevic Sephton S, Mu L, Schweizer WB, Schibli R, Krämer SD, Ametamey SM. Synthesis and evaluation of novel alpha-fluorinated (E)-3-((6-methylpyridin-2-yl)ethynyl)cyclohex-2-enone-O-methyl oxime (ABP688) derivatives as metabotropic glutamate receptor subtype 5 PET radiotracers. *J Med Chem.* 2012;55:7154-7162.

11. Chu UB, Ruoho AE. Sigma receptor binding assays. *Curr Protoc Pharmacol.* 2015;71:1 34 31-21.

12. Nguyen VH, Kassiou M, Johnston GA, Christie MJ. Comparison of binding parameters of sigma 1 and sigma 2 binding sites in rat and guinea pig brain membranes: novel subtype-selective trishomocubanes. *Eur J Pharmacol.* 1996;311:233-240.

13. Langa F, Codony X, Tovar V, et al. Generation and phenotypic analysis of sigma receptor type I (sigma 1) knockout mice. *Eur J Neurosci.* 2003;18:2188-2196.

14. Müller Herde A, Keller C, Milicevic Sephton S, et al. Quantitative positron emission tomography of mGluR5 in rat brain with [(18) F]PSS232 at minimal invasiveness and reduced model complexity. *J Neurochem.* 2015;133:330-342.

15. Goertzen AL, Bao Q, Bergeron M, et al. NEMA NU 4-2008 comparison of preclinical PET imaging systems. *J Nucl Med.* 2012;53:1300-1309.

16. Ginovart N, Sun W, Wilson AA, Houle S, Kapur S. Quantitative validation of an intracerebral beta-sensitive microprobe system to determine in vivo drug-induced receptor occupancy using [11C]raclopride in rats. *Synapse.* 2004;52:89-99.

17. Krämer SD. Positron Emission Tomography (PET): Quantification and Kinetic Modeling. *Reference Module in Chemistry, Molecular Sciences and Chemical Engineering*. Amsterdam (NL): Elsevier; 2015.

18. Innis RB, Cunningham VJ, Delforge J, et al. Consensus nomenclature for in vivo imaging of reversibly binding radioligands. *J Cereb Blood Flow Metab.* 2007;27:1533-1539.

19. Logan J, Fowler JS, Volkow ND, et al. Graphical analysis of reversible radioligand binding from time-activity measurements applied to [N-11C-methyl]-(-)-cocaine PET studies in human subjects. *J Cereb Blood Flow Metab.* 1990;10:740-747.

20. Hurvich CM, Tsai C-L. Regression and time series model selection in small samples. *Biometrika.* 1989;76:297-307.

21. Malherbe P, Mutel V, Broger C, et al. Identification of critical residues in the amino terminal domain of the human NR2B subunit involved in the RO 25-6981 binding pocket. *J Pharmacol Exp Ther.* 2003;307:897-905.

22. Gitto R, De Luca L, Ferro S, et al. Synthesis and biological characterization of 3-substituted-1H-indoles as ligands of GluN2B-containing N-methyl-D-aspartate receptors. *J Med Chem.* 2011;54:8702-8706.

23. Chu UB, Ruoho AE. Biochemical pharmacology of the sigma-1 receptor. *Mol Pharmacol.* 2016;89:142-153.

24. Lorrain DS, Baccei CS, Bristow LJ, Anderson JJ, Varney MA. Effects of ketamine and N-methyl-D-aspartate on glutamate and dopamine release in the rat prefrontal cortex: modulation by a group II selective metabotropic glutamate receptor agonist LY379268. *Neuroscience.* 2003;117:697-706.

25. Cunningham VJ, Rabiner EA, Slifstein M, Laruelle M, Gunn RN. Measuring drug occupancy in the absence of a reference region: the Lassen plot re-visited. *J Cereb Blood Flow Metab.* 2010;30:46-50.

26. Higley MJ, Sabatini BL. Competitive regulation of synaptic Ca2+ influx by D2 dopamine and A2A adenosine receptors. *Nat Neurosci.* 2010;13:958-966.

27. Zhang XJ, Liu LL, Jiang SX, Zhong YM, Yang XL. Activation of the sigma receptor 1 suppresses NMDA responses in rat retinal ganglion cells. *Neuroscience.* 2011;177:12-22.

28. Suzuki T, Suganuma T, Nishino J, Hanano M. Pharmacokinetics of pentazocine and its occupancy of opioid receptors in rat brain. *Biol Pharm Bull.* 1997;20:1193-1198.

29. Sasaki S, Kurosaki F, Haradahira T, et al. Synthesis of 11C-labelled bis(phenylalkyl)amines and their in vitro and in vivo binding properties in rodent and monkey brains. *Biol Pharm Bull.* 2004;27:531-537.

30. Roger G, Lagnel B, Besret L, et al. Synthesis, radiosynthesis and in vivo evaluation of 5-[3-(4-benzylpiperidin-1-yl)prop-1-ynyl]-1,3-dihydrobenzoimidazol-2-[(11)C]one, as a potent NR(1A)/2B subtype selective NMDA PET radiotracer. *Bioorg Med Chem.* 2003;11:5401-5408.

31. Arstad E, Platzer S, Berthele A, et al. Towards NR2B receptor selective imaging agents for PET-synthesis and evaluation of N-[11C]-(2-methoxy)benzyl (E)-styrene-, 2-naphthyl- and 4-trifluoromethoxyphenylamidine. *Bioorg Med Chem.* 2006;14:6307-6313.

32. Labas R, Gilbert G, Nicole O, et al. Synthesis, evaluation and metabolic studies of radiotracers containing a 4-(4-[18F]-fluorobenzyl)piperidin-1-yl moiety for the PET imaging of NR2B NMDA receptors. *Eur J Med Chem.* 2011;46:2295-2309.

33. Koudih R, Gilbert G, Dhilly M, et al. Synthesis and in vitro characterization of trans- and cis-[(18)F]-4-methylbenzyl 4-[(pyrimidin-2-ylamino)methyl]-3-fluoropiperidine-1-carboxylates as new potential PET radiotracer candidates for the NR2B subtype N-methyl-D-aspartate receptor. *Eur J Med Chem.* 2012;53:408-415.

34. Christiaans JA, Klein PJ, Metaxas A, et al. Synthesis and preclinical evaluation of carbon-11 labelled N-((5-(4-fluoro-2-[(11)C]methoxyphenyl)pyridin-3-yl)methyl)cyclopentanamine as a PET tracer for NR2B subunit-containing NMDA receptors. *Nucl Med Biol.* 2014;41:670-680.

35. Mutel V, Buchy D, Klingelschmidt A, et al. In vitro binding properties in rat brain of [3H]Ro 25-6981, a potent and selective antagonist of NMDA receptors containing NR2B subunits. *J Neurochem.* 1998;70:2147-2155.

36. Akazawa C, Shigemoto R, Bessho Y, Nakanishi S, Mizuno N. Differential expression of five N-methyl-D-aspartate receptor subunit mRNAs in the cerebellum of developing and adult rats. *J Comp Neurol.* 1994;347:150-160.

37. Jin DH, Jung YW, Ko BH, Moon IS. Immunoblot analyses on the differential distribution of NR2A and NR2B subunits in the adult rat brain. *Mol Cells.* 1997;7:749-754.

38. Haradahira T, Maeda J, Okauchi T, et al. Synthesis, in vitro and in vivo pharmacology of a C-11 labeled analog of CP-101,606, (+/-)threo-1-(4-hydroxyphenyl)-2-[4-hydroxy-4-(p-[11C]methoxyphenyl)piperidino]-1 -propanol, as a PET tracer for NR2B subunit-containing NMDA receptors. *Nucl Med Biol.* 2002;29:517-525.

39. Hinoi E, Fujimori S, Nakamura Y, et al. Constitutive expression of heterologous N-methyl-D-aspartate receptor subunits in rat adrenal medulla. *J Neurosci Res.* 2002;68:36-45.

40. Ibarrola D, Seegers H, Jaillard A, Hommel M, Decorps M, Massarelli R. The effect of eliprodil on the evolution of a focal cerebral ischaemia in vivo. *Eur J Pharmacol.* 1998;352:29-35.

41. Hogg S, Perron C, Barneoud P, Sanger DJ, Moser PC. Neuroprotective effect of eliprodil: attenuation of a conditioned freezing deficit induced by traumatic injury of the right parietal cortex in the rat. *J Neurotrauma.* 1998;15:545-553.

42. Balasuriya D, Stewart AP, Edwardson JM. The sigma-1 receptor interacts directly with GluN1 but not GluN2A in the GluN1/GluN2A NMDA receptor. *J Neurosci.* 2013;33:18219-18224.

43. Liu XY, Chu XP, Mao LM, et al. Modulation of D2R-NR2B interactions in response to cocaine. *Neuron.* 2006;52:897-909.

44. Leveque JC, Macias W, Rajadhyaksha A, et al. Intracellular modulation of NMDA receptor function by antipsychotic drugs. *J Neurosci.* 2000;20:4011-4020.

45. Colabufo NA, Berardi F, Contino M, et al. Antiproliferative and cytotoxic effects of some sigma2 agonists and sigma1 antagonists in tumour cell lines. *Naunyn Schmiedebergs Arch Pharmacol.* 2004;370:106-113.

46. Esaki T, Itoh Y, Shimoji K, Cook M, Jehle J, Sokoloff L. Effects of dopamine receptor blockade on cerebral blood flow response to somatosensory stimulation in the unanesthetized rat. *J Pharmacol Exp Ther.* 2002;303:497-502.

47. Spargo PM, Howard WV, Saunders DA. Sedation and cerebral angiography. The effects of pentazocine and midazolam on arterial carbon dioxide tension. *Anaesthesia.* 1985;40:901-903.

FIGURE LEGENDS

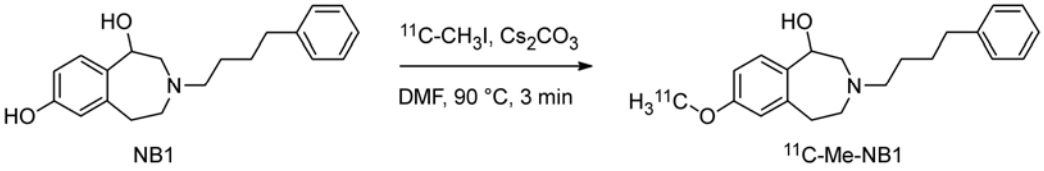

FIGURE 1. Radiosynthesis of ^{11}C-Me-NB1

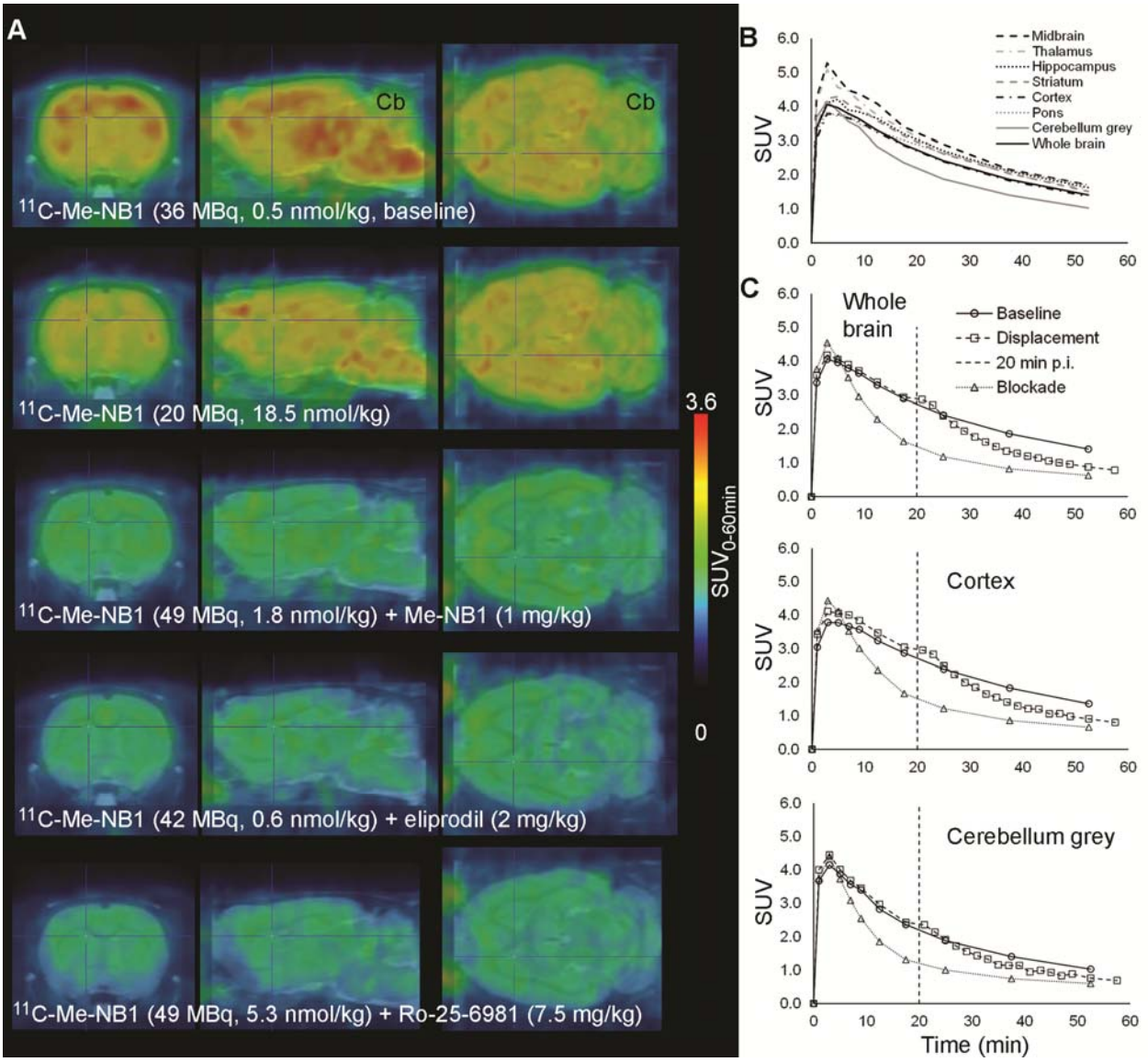

FIGURE 2. **A**) Rat brain ^{11}C-Me-NB1 PET images (0-60 min), superimposed on a MRI template (PMOD). Cb, cerebellum. **B**) Brain region TACs of a baseline scan (67 MBq; 2.1 nmol/kg; 394 g). **C**) TACs under baseline conditions (○, as in **B**), or with 1 mg/kg eliprodil i.v. 1 min before ^{11}C-Me-NB1 (Δ, blockade, 35 MBq, 0.44 nmol/kg, 370 g) or 20 min after ^{11}C-Me-NB1 injection (□, displacement, 55 MBq, 0.57 nmol/kg, 449 g). Brain regions as indicated. Vertical broken line, time point of eliprodil i.v. injection for displacement.

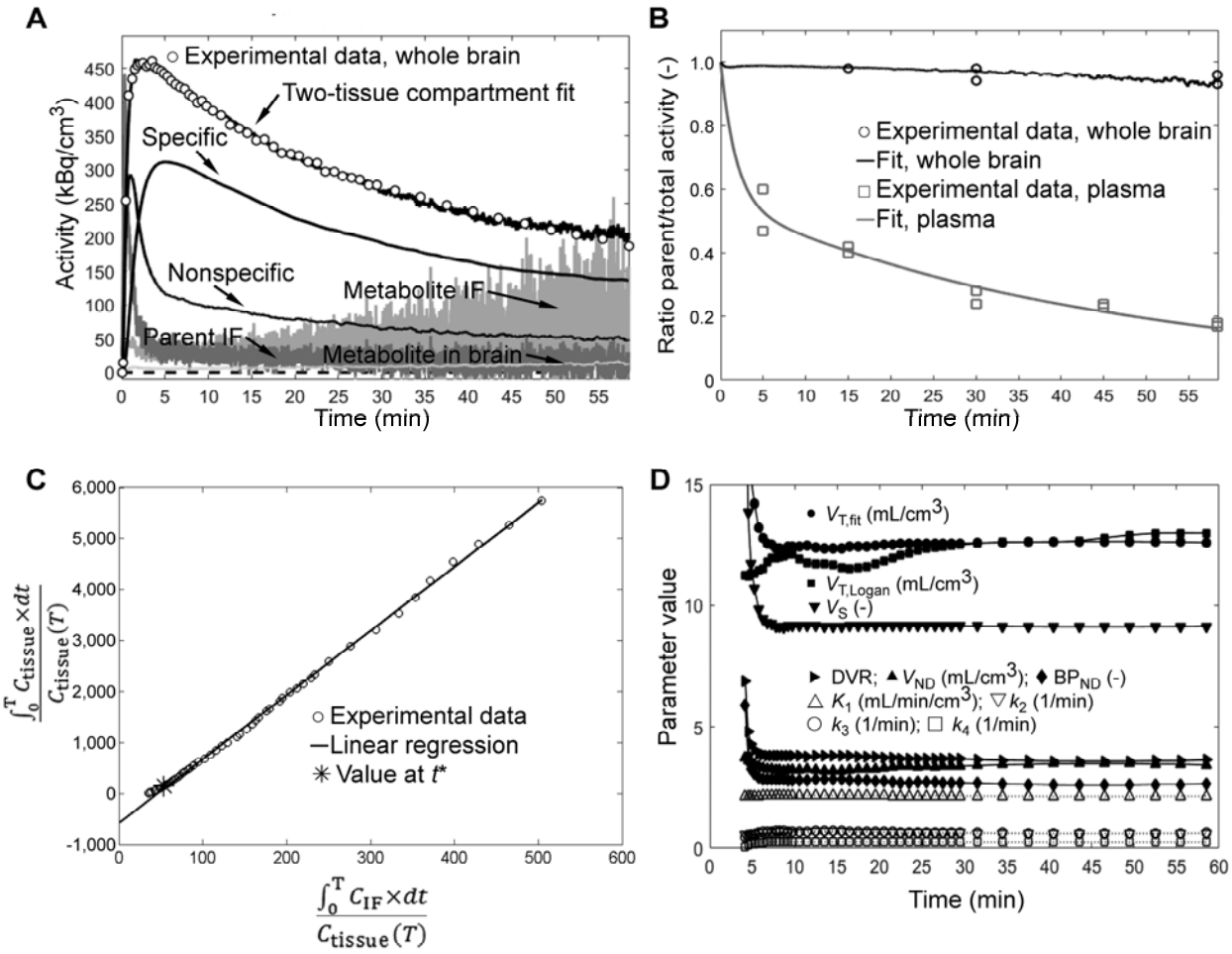

FIGURE 3. ^{11}C-Me-NB1 kinetic evaluation in rat whole brain. Representative baseline scan (31.8 MBq; 0.44 nmol/kg; 321 g). **A**) Whole brain TAC (○) and input functions (IF) as indicated. Black lines, fit results as indicated. 100 kBq/cm^3 corresponds to ~ 0.4 nM ^{11}C-Me-NB1. $V_{T,fit}$=12.6 mL/cm^3. **B**) Experimental and fit ratios of parent tracer/total radioactivity in plasma and brain, as indicated. Residuals from the experimental TAC and ratios parent/total radioactivity were minimized simultaneously during the fitting procedure. **C**) Logan plot. Plasma and brain TACs were corrected for the fit ratios parent tracer/total radioactivity. $V_{T,Logan}$=12.5 mL/cm^3. ○, experimental data; line, linear regression of data with t > 3 min. C_{tissue}, radioactivity in the tissue (image data); C_{IF}, radioactivity in the arterial plasma; T, time points. **D**) Fit parameters (as indicated) for scan durations between 4 and 60 min.

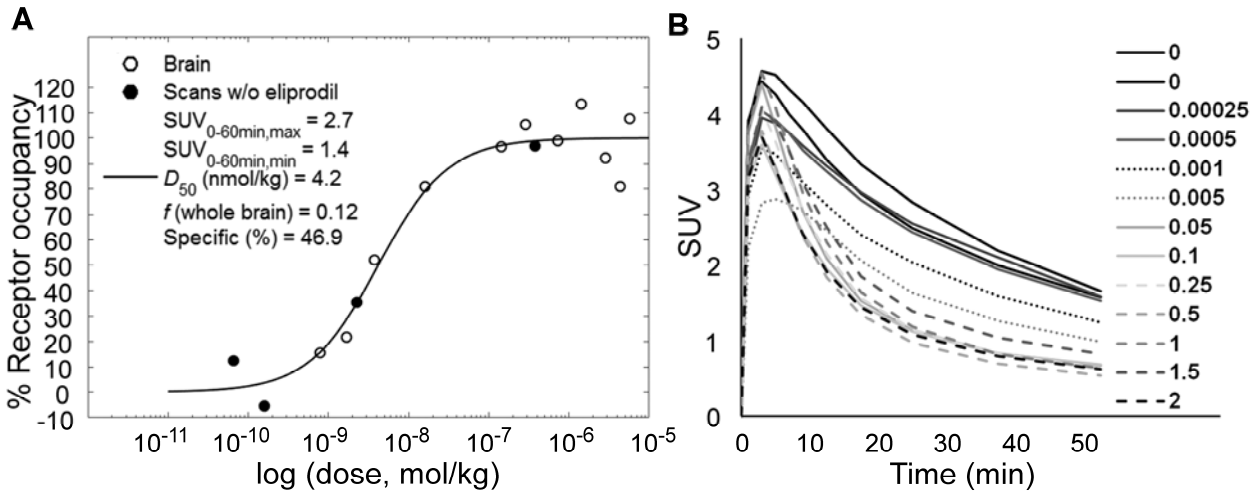

FIGURE 4. **A**) Rat whole brain NTD binding site occupancy by eliprodil. ○, ^{11}C-Me-NB1 with eliprodil; ●, ^{11}C-Me-NB1/Me-NB1 alone. Receptor occupancy by ^{11}C-Me-NB1 and Me-NB1 was included in the saturation function (Methods). $SUV_{0\text{-}60min}$ were fitted to a saturation function and data was transformed to % receptor occupancy. Solid line, transformed fit. **B**) Respective TACs, eliprodil doses are indicated in mg/kg.

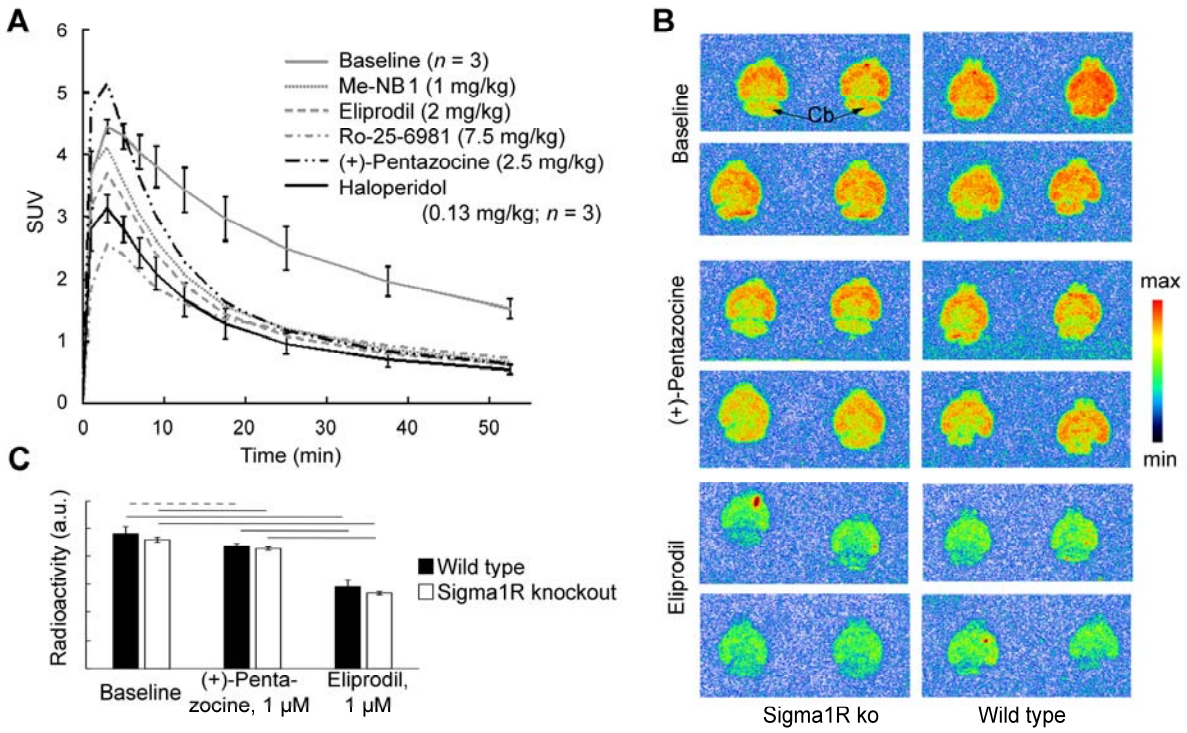

FIGURE 5. Influence of (+)-pentazocine and haloperidol on ^{11}C-Me-NB1 PET in rat brain (**A**) and *in vitro* autoradiography with brain slices of S1R knockout (ko) mice (**B,C**). **A**) TACs after drug administration as indicated. TACs after blocking with Me-NB1, eliprodil and Ro-25-6981 are shown for comparison. SUV within the first few minutes may be affected by drug-induced changes in cerebral blood flow (*46,47*), and increased plasma levels under blocking conditions (**Fig. 3**). **B**) ^{11}C-Me-NB1 autoradiograms of brain slices from Sigma1R knockout and wild type mice as indicated. Incubation with 4.0 nM ^{11}C-Me-NB1 alone (baseline) or together with (+)-pentazocine or eliprodil. **C**) Quantitative analysis of the autoradiograms in **B.** No significant difference between wild type and Sigma1R knockout mice for all 3 conditions ($p > 0.05$). (+)-Pentazocine (1 µM) reduced ^{11}C-Me-NB1 binding in wildtype and Sigma1R ko mice by < 10%. The reduction by an equal concentration of eliprodil was 40 and 42 %, respectively (horizontal broken line, $p < 0.05$; solid lines, $p < 0.01$). a.u., arbitrary units.

Supplemental Figures

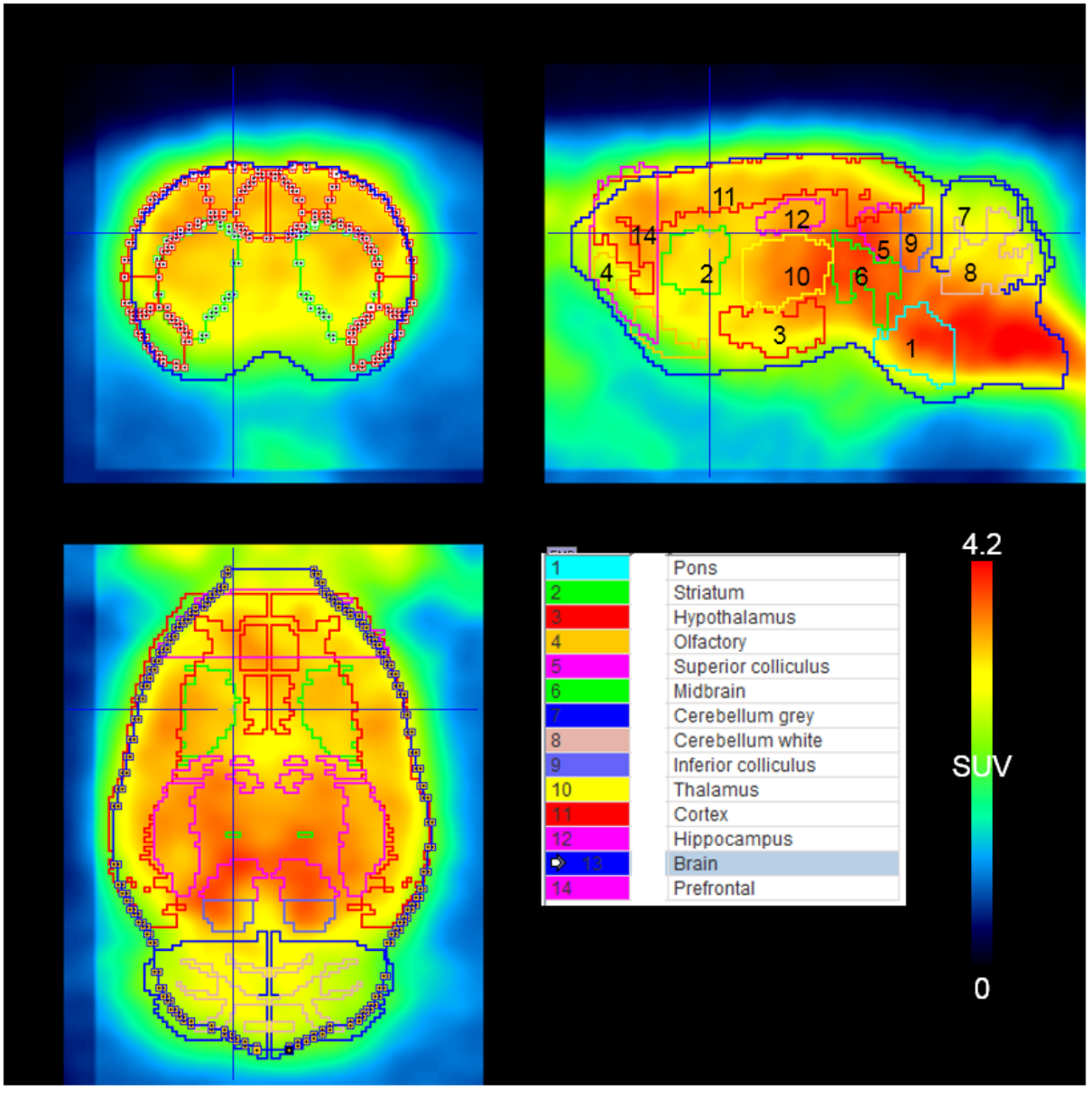

Supplemental Figure 1. ^{11}C-Me-NB1 PET images of rat brain, averaged from 3 individual scans, 0 to 60 min after tracer injection. PET data were reconstructed with 2D Fourier rebinning/ordered-subsets expectation maximization algorithms (FORE/OSEM), 2 iterations, 16 subsets, into time frames between 20 and 180 s for kinetic modelling with an input function or between 120 and 300 s for scans without an input function. PET data were corrected for singles and randoms but not for attenuation. The brain region template used for the quantitative analysis is superimposed (PMOD). The volumes (mm^3) of the individual regions of interest were pons, 45; striatum, 87; hypothalamus, 37; olfactory, 28; superior colliculus, 14; midbrain, 23; cerebellum grey matter, 150; cerebellum white matter, 47; inferior colliculus, 11; thalamus, 61; cortex, 576; hippocampus, 70; whole brain, 1831; prefrontal cortex, 132. The standardized uptake values (SUV) were calculated as Bq per g tissue divided by injected Bq per g body weight. The SUV corresponds to % injected dose per g tissue multiplied with body weight (g) and divided by 100 %. Specific binding in % in the *ex vivo* biodistribution experiments were calculated as (SUV(baseline)-SUV(blockade))/SUV(baseline)*100.

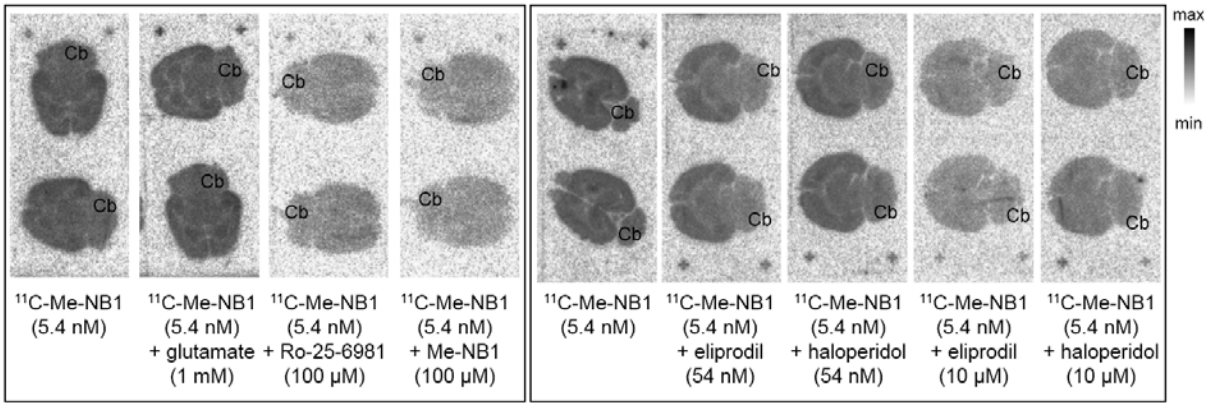

Supplemental Figure 2. Characterization of ^{11}C-Me-NB1 binding to rat brain tissue by *in vitro* autoradiography. Baseline and blocking conditions as indicated. Results from two independent experiments as indicated by the frames. Cb, cerebellum, for orientation. Intensity bar with maximal (max) and minimal (min) unmodified phosphorimager signal intensity (a.u.). Horizontal rat brain slices (20 µm) of adult male Wistar rats were incubated for 30 min at room temperature with ^{11}C-Me-NB1 alone or in combination with the indicated compounds, in HEPES buffer (30 mM HEPES, 110 mM NaCl, 5 mM KCl, 2.5 mM $CaCl_2$, 1.2 mM $MgCl_2$, pH 7.4) containing 0.1 % bovine serum albumin (HEPES/BSA). After incubation, the slices were washed with HEPES/BSA (8 min), HEPES buffer (2×3 min) and water (2×5 s). The dried slices were exposed for 20 min to a phosphorimager plate and read in a phosphorimager BAS5000 (Fuji, Tokyo, Japan; software AIDA v4.5). Radioactivity accumulation was quantified with the software PMOD v3.7 (PMOD Technologies, Zurich, Switzerland). Note that the bivalent cations in the HEPES buffer could affect ^{11}C-Me-NB1 binding (*1*).

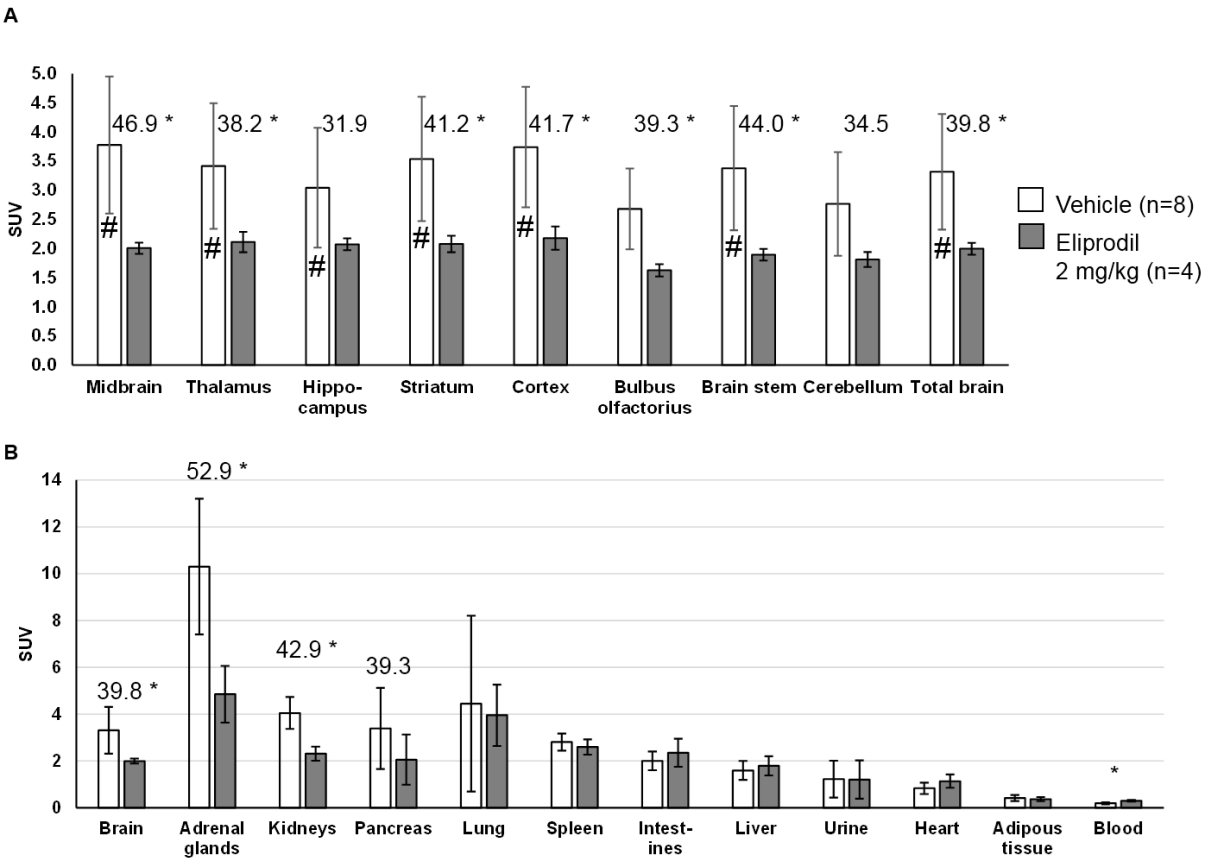

Supplemental Figure 3. Distribution of ^{11}C-Me-NB1 in rat tissues determined by dissection 15 min after ^{11}C-Me-NB1 i.v. injection under baseline and blocking conditions, as indicated. Numbers show the percent specific binding. * indicates significant reduction (increase in the case of blood) by eliprodil ($p < 0.05$). # indicates significantly higher SUV than cerebellum under baseline conditions ($p < 0.01$, paired t-test, not corrected for multiple comparisons). **A**) Brain regions. **B**) All tissues, including whole brain (calculated from the SUV and tissue weights in **A**).

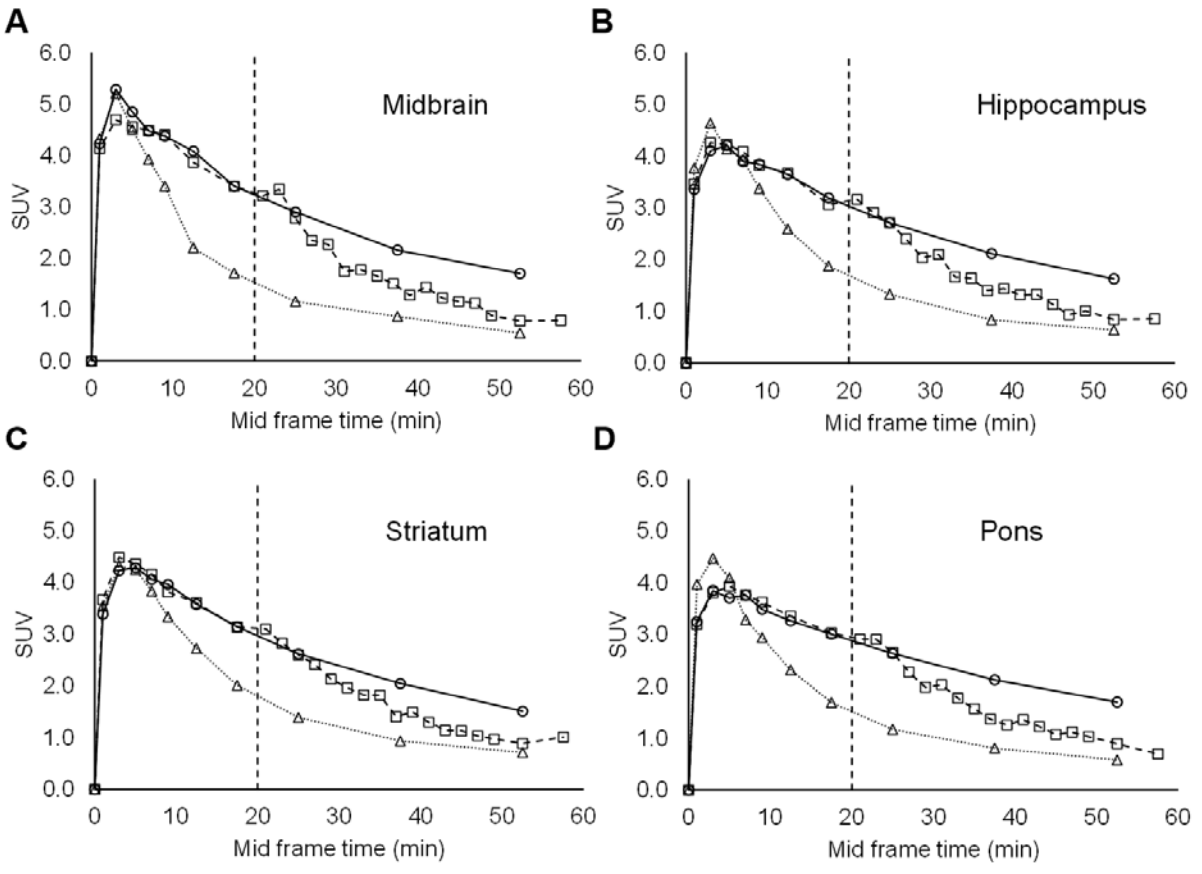

Supplemental Figure 4. Brain region TACs of ^{11}C-Me-NB1 under baseline, blocking and displacement conditions. Same scans and conditions as shown in **Fig. 2**. ○, Baseline; △, blockade with 1 mg/kg eliprodil (1 min before tracer injection); □, displacement with 1 mg/kg eliprodil (20 min after tracer injection, indicated by vertical broken lines). **A**) Midbrain, **B**) hippocampus, **C**) striatum, **D**) pons.

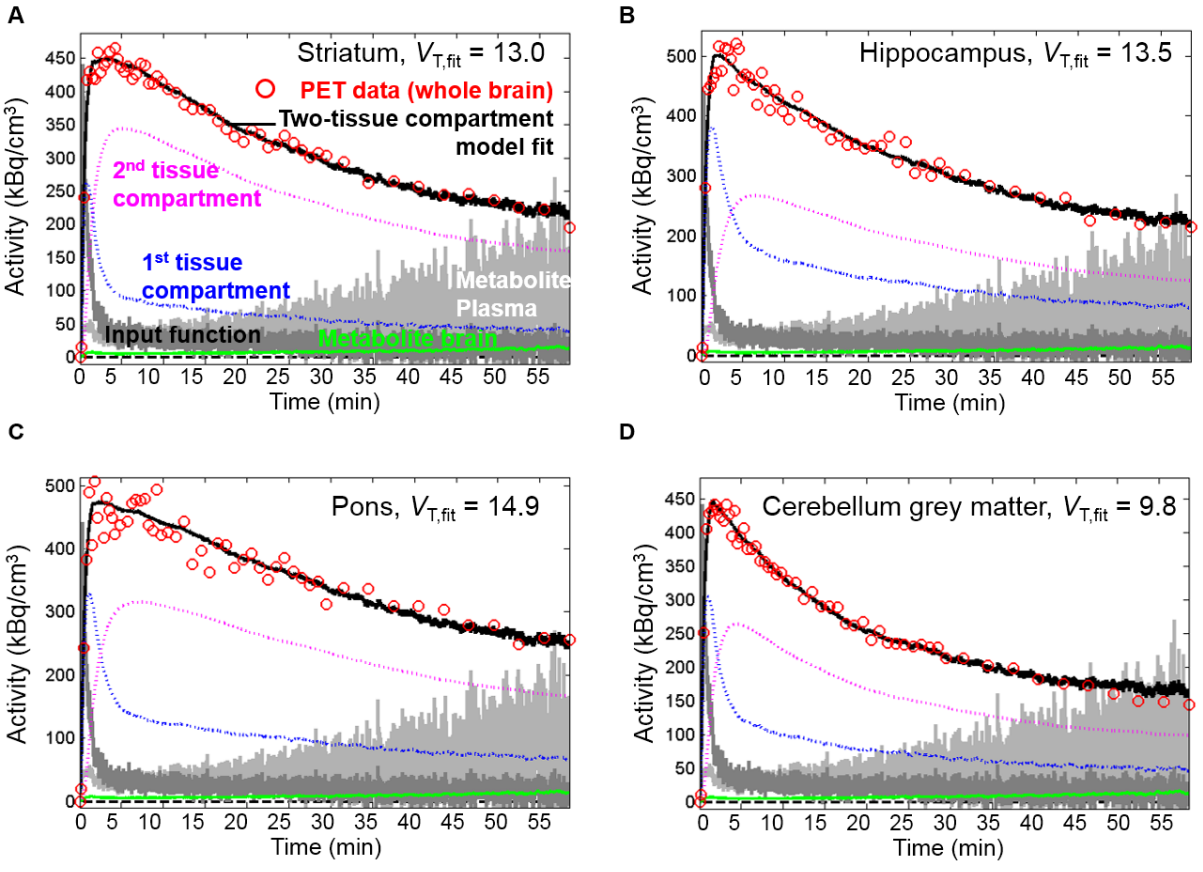

Supplemental Figure 5. ^{11}C-Me-NB1 TACs and kinetic modeling for individual brain regions of the scan shown in **Fig. 3**. **A**) Striatum, **B**) hippocampus, **C**) pons, **D**) cerebellum grey matter. ○, experimental data; lines, dark grey, input function; light grey, input function of radiometabolite; black solid, fit TAC; pink dotted, tracer simulated in 2nd tissue compartment (specific binding); blue dotted, tracer simulated in 1st tissue compartment (non-displaceable); green, radiometabolite simulated in brain. The respective $V_{T,fit}$ (mL/cm^3) are shown in the panels. Ratio parent/total radioactivity in plasma and brain: in a pilot experiment, a rat (339 g) was injected into a lateral tail vein 81.8 MBq ^{11}C-Me-NB1 under isoflurane anesthesia and sacrificed 5 min later by decapitation under anesthesia. The blood was collected and plasma was separated by centrifugation (5000 × g, 5 min, 4°C). The brain was homogenized in an equivalent volume of ice cold PBS for 1-2 min. The proteins in both samples were precipitated with equivalent volumes of ice cold acetonitrile and centrifugation as above. The analysis of the filtered supernatants by TLC (silica gel, MERCK KGaA; mobile phase, methanol) and the phosphorimager revealed a single, polar radiometabolite beside the parent tracer. To determine the ratio of parent tracer to total radioactivity in plasma and brain over time, 6 rats (227-421 g) were injected into a lateral tail vein with 28-37 MBq ^{11}C-Me-NB1 and blood samples were drawn from the opposite vein at the indicated time points. The rats were sacrificed at 15, 30 and 60 min, respectively, and brains and blood were collected. Blood and brain samples were processed as above. The unfiltered supernatants after acetonitrile addition were diluted with 3 volumes of water. The solution was passed through a Sep-Pak C18 Light cartridge (Waters, Milford, MA) and washed with 1 mL water. The combined aqueous phase contained the polar radiometabolite. The parent compound was eluted with 1 mL ethanol. The separation was confirmed by TLC. The radioactivity in both aqueous and ethanol eluents was quantified in the gamma counter and the ratio parent to total radioactivity was calculated as the radioactivity in the ethanol phase divided by the sum of the radioactivity in both

phases. The ratio of plasma to whole blood radioactivity was determined from plasma and whole blood in the gamma counter, it was 1.11. Kinetic modeling: Scans with an input function were analyzed based on a two-tissue compartment model (*2*) with a home-written MATLAB script (MathWorks, Natick, MA). PET TACs and not-decay corrected blood coincidences were loaded. The start time of the blood coincidences curve and the background coincidences were estimated as the time point of the first significant increase in the data and the average counts before this time point, respectively. Both values were refined during the fitting procedure. The background- and start time-corrected coincidences were decay-corrected and multiplied with the experimentally determined calibration factor between the PET scanner and the coincidence counter and the plasma/blood radioactivity ratio of 1.11. They were further multiplied with a bi-exponential function (refined during the fitting procedure) to correct for the experimentally determined ratio parent/total radioactivity in plasma and the radiometabolite input function was revealed as the difference between the total and parent coincidences. These adapted input functions were convoluted with the weighting function for a two-tissue compartment model for the parent tracer, defined by K_1, k_2, k_3 and k_4, and a one-tissue compartment model for the radiometabolite, defined by K_{1M} and k_{2M} (*2*). The squared residuals between the experimental data and the fit functions for the brain TAC (consisting of parent tracer, radiometabolite and blood radioactivity, assuming a partial volume of 5 % blood in the brain), as well as fit functions for the parent/total radioactivity in plasma and brain were minimized with the function fmincon and a multistart procedure with 64 runs. For whole brain, the difference between $V_{T,fit}$ and $V_{T,Logan}$, determined from the Logan plot (*3*), were furthermore minimized to allow to accurately define the starting time and background coincidences of the blood coincidence curve. In addition, the 4 parameters defining the ratio parent/total radioactivity in plasma were fit. In summary, the following parameters were fit simultaneously: K_1, k_2, k_3, k_4, input function start time, blood coincidence background, A, B, a and b of the function parent/total radioactivity in plasma = $A\times\exp(-a\times t)+B\times\exp(-b\times t)+(1-A-B)$, furthermore K_{1M} and k_{2M}. The parameters were fit by minimizing the differences between the fit and experimental brain TAC, the fit and experimental plasma and brain ratios parent tracer/total radioactivity and the $V_{T,fit}$ and $V_{T,Logan}$. The resulting start time and background coincidences of the blood coincidence curve and the bi-exponential function defining the parent/total radioactivity ratio in plasma were then fixed to analyze the stability of K_1 to k_4 and the composite parameters for whole brain at truncated scan durations and for the individual brain regions at full scan time, in 8 runs each (multistart with fmincon). For comparison, K_{1M} was fixed at 0, ignoring radiometabolite distribution to the brain.

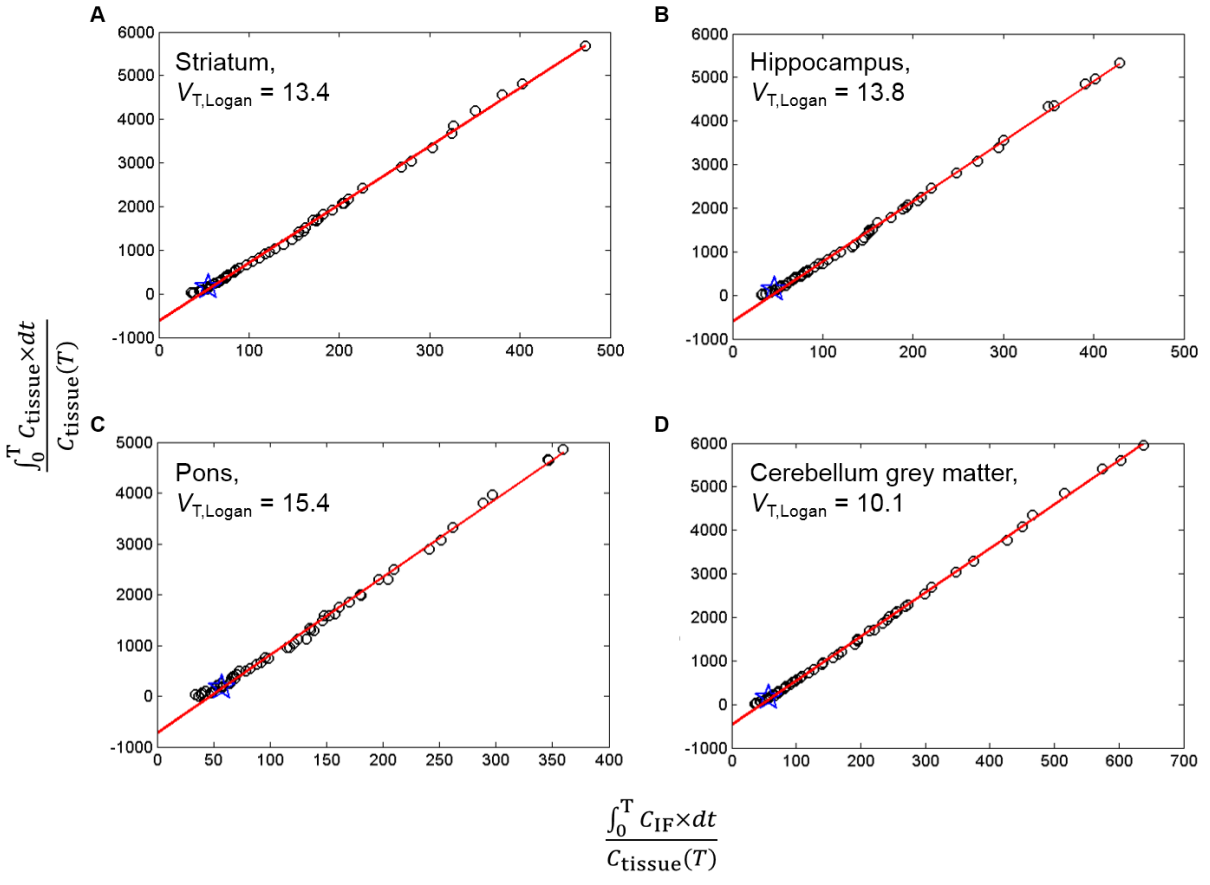

Supplemental Figure 6. Logan plots for individual brain regions of the scan shown in **Figure 3** and **Supplemental Figure 5**. **A**) Striatum, **B**) hippocampus, **C**) pons, **D**) cerebellum grey matter. Symbols and lines as indicated in **Figure 3** in the manuscript. The respective $V_{T,Logan}$ (mL/cm^3) are shown in the panels.

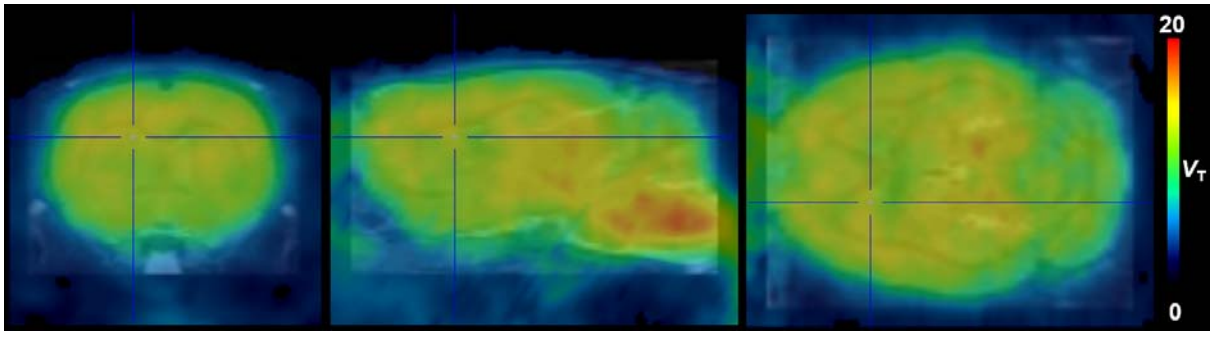

Supplemental Figure 7. Parametric maps for V_T (mL/cm^3) for the scan shown in **Fig. 2A**. The maps were generated with PMOD v3.8 based on the input function (see above) and the image data. Vertical (left), sagittal (middle), horizontal (right) planes at 1.7 mm (left-right), 3.8 mm (dorsal-ventral), 0.4 mm (anterior-posterior) from Bregma (as in **Fig. 2A**).

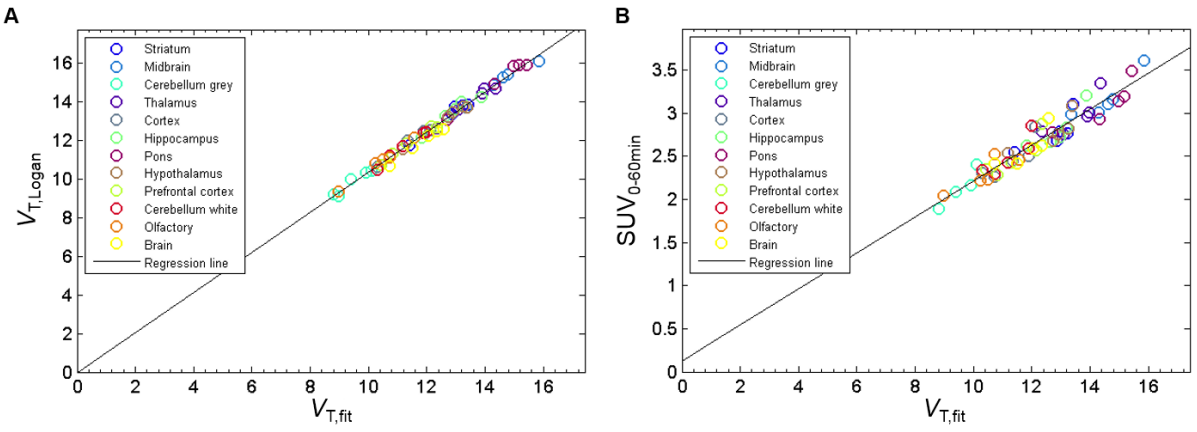

Supplemental Figure 8. Comparison of $V_{T,Logan}$ and $SUV_{0-60min}$ with $V_{T,fit}$. **A**) $V_{T,Logan}$ *vs* $V_{T,fit}$ of 5 scans and 12 brain regions each. The correlation was $V_{T,Logan} = 1.04 \times V_{T,fit} - 0.03$ mL/cm^3 ($r^2 = 0.99$). **B**) $SUV_{0-60min}$ *vs* $V_{T,fit}$ (same scans and regions as in **A**). The correlation was $SUV_{0-60min} = (0.209$ cm^3/mL$) \times V_{T,fit} + 0.123$; $r^2 = 0.913$.

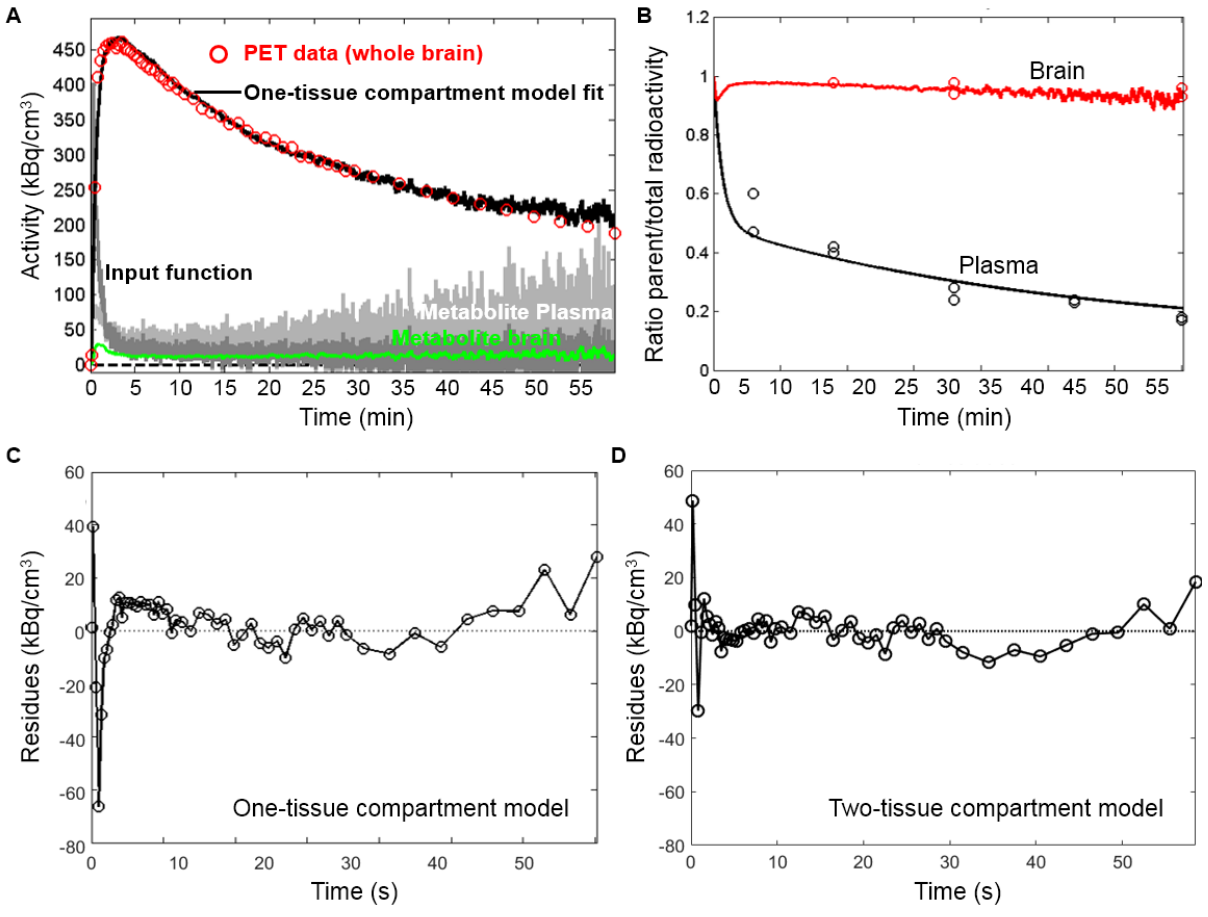

Supplemental Figure 9. The experimental brain TAC shown in **Fig. 3** fit to one-tissue compartment models for both the parent tracer and the radiometabolite. **A**) Fit brain TAC. **B**) Simultaneously fit ratios parent tracer to total radioactivity in brain and plasma. **C**) Residuals for the brain TAC fit with a one-tissue compartment model each for parent tracer and radiometabolite. The corrected Akaike information criterion was 317.9. **D**) Residuals for the brain TAC fit with a two-tissue compartment model for the parent tracer and a one-tissue compartment model for the radiometabolite (residuals from fit shown in **Fig. 3A**), The Akaike information criterion was 266.1. Deviations from the experimental parent/total radioactivity ratios in plasma and brain were not included in the calculations of the Akaike information criterion. The model with the lower Akaike information criterion is the preferred model.

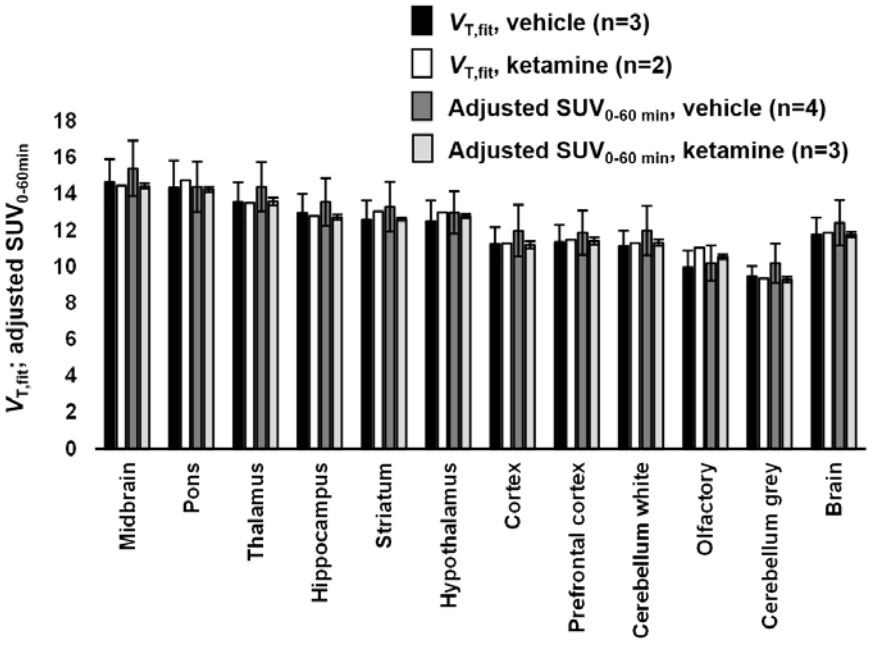

Supplemental Figure 10. Quantitative PET with and without an input function and influence of ketamine on ^{11}C-Me-NB1 PET. $V_{T,fit}$ values (mL/cm^3) from kinetic modeling and adjusted $SUV_{0-60min}$ as ($SUV_{0-60min}$-0.123)/(0.209 cm^3/mL), according to **Supplemental Figure 8B**. Scans without a meaningful input function were included for the adjusted $SUV_{0-60min}$. Mean values with standard deviations (for $n \geq 3$), n as indicated. To study the influence of ketamine and glutamate *in vivo*, 3 of the 7 rats with input-function recording were administered intraperitoneally 25 mg/kg ketamine 30 min before tracer injection. The $V_{T,fit}$ values of the 2 ketamine-treated rats with complete input function were within the standard deviations of the respective values from the baseline scans or close to this range (**Supplemental Tables 3 and 4**) and no significant difference was detected between the respective $SUV_{0-60min}$ values. This excludes a major influence of the ketamine challenge on ^{11}C-Me-NB1 accumulation in rat brain under isoflurane anesthesia. $V_{T,fit}$ and adjusted SUV of all brain regions except olfactory bulb were significantly higher than the respective parameter of cerebellum grey matter ($p < 0.05$, paired t-test, not corrected for multiple comparisons and not analyzed for $n < 3$).

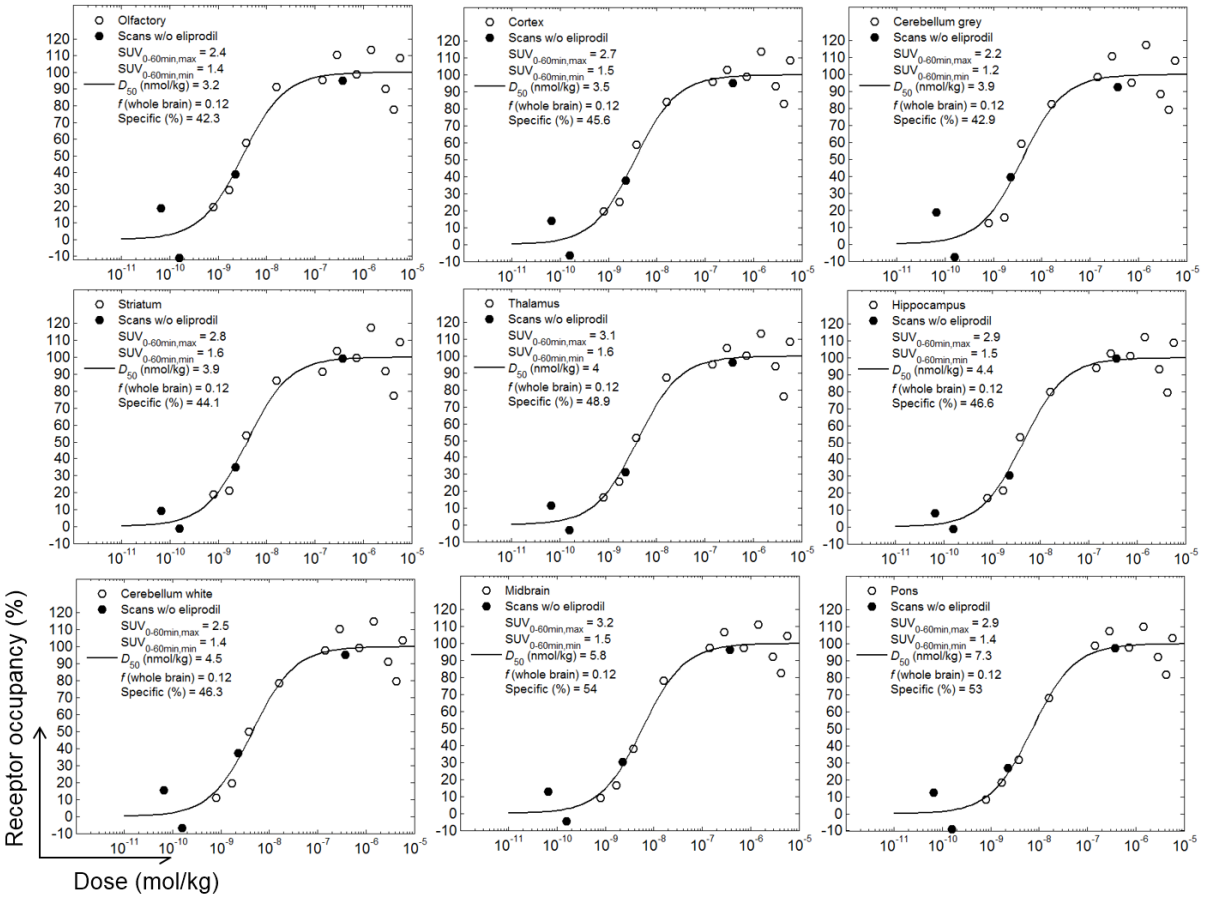

Supplemental Figure 11. Receptor occupancy by eliprodil as determined by PET with ^{11}C-Me-NB1 in individual brain regions as indicated. The regions and fit parameters are indicated in the panels.

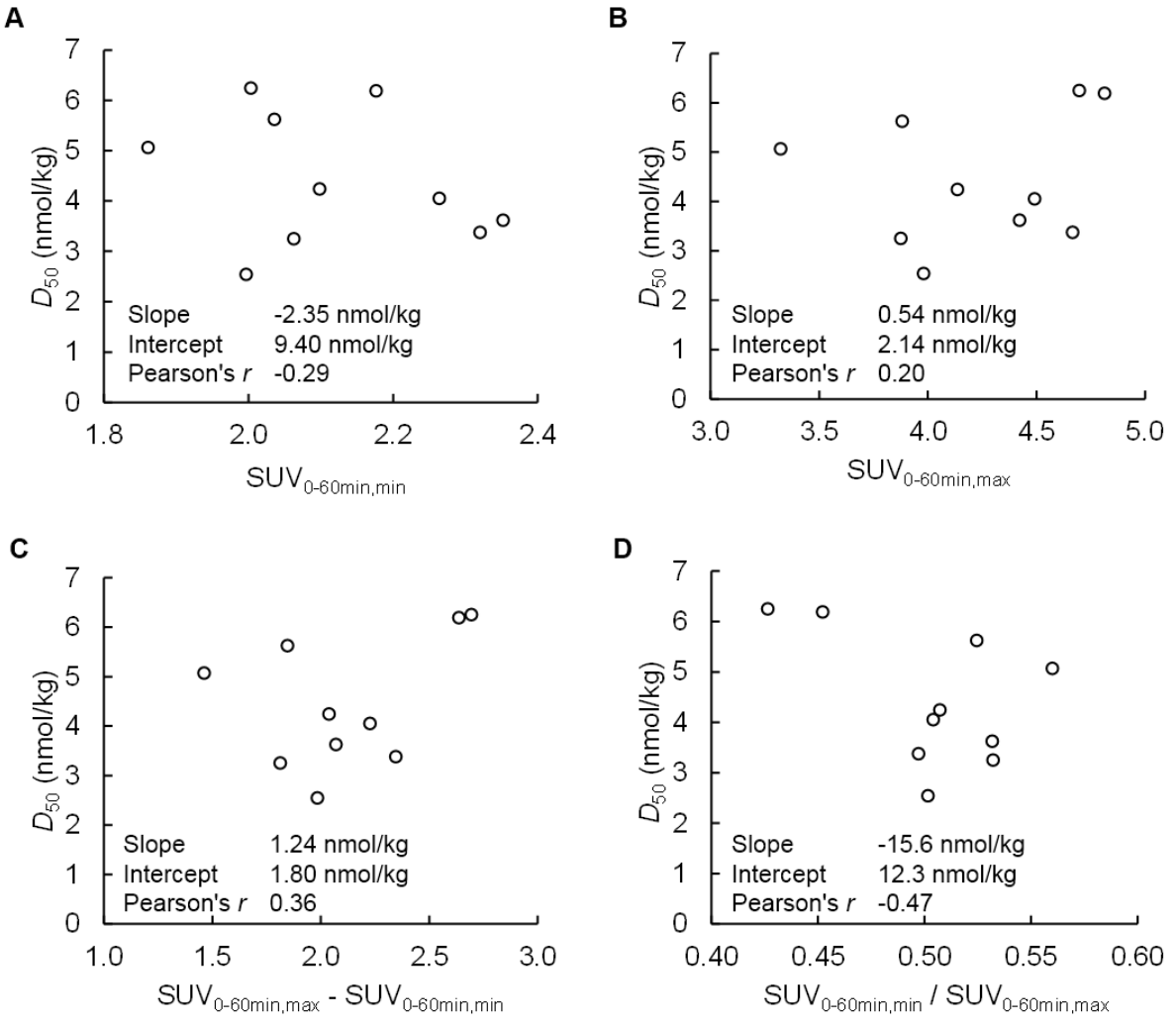

Supplemental Figure 12. Weak or absent correlation between D_{50} and fitted non-displaceable tracer accumulation ($SUV_{0\text{-}60min,min}$). $SUV_{0\text{-}60min,max}$ and $SUV_{0\text{-}60min,min}$ are the fitted maximal and minimal $SUV_{0\text{-}60min}$ of the receptor occupancy data of the various brain regions (**Fig. 4** and **Supplemental Fig. 11**). **A**) D_{50} *vs* $SUV_{0\text{-}60min,min}$. **B**) D_{50} *vs* $SUV_{0\text{-}60min,max}$. **C**) D_{50} *vs* $SUV_{0\text{-}60min}$ of specifically bound tracer. **D**) D_{50} *vs* the relative $SUV_{0\text{-}60min,min}$. Linear regression analysis results are shown in the panels.

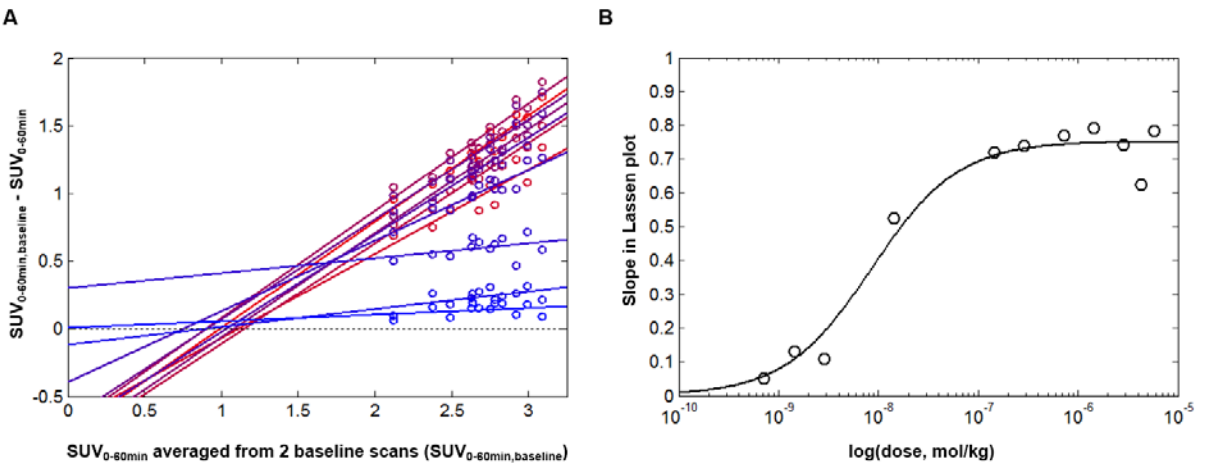

Supplemental Figure 13. Receptor occupancy estimated from the Lassen plot. **A**) Lassen plot according to Cunningham et al. (*4*). $SUV_{0\text{-}60min,baseline}$ was averaged from the two baseline scans with the lowest ^{11}C-Me-NB1 dose in nmol/kg, i.e., 0.5 and 1.3 nmol/kg (x-axis). The differences between the averaged regional baseline $SUV_{0\text{-}60min}$ values and the regional $SUV_{0\text{-}60min}$ values after eliprodil administration are plotted on the y-axis (increasing eliprodil dose from blue to red color). Under ideal conditions, the slope of the Lassen plot (symbols, linear regression of the data points at a particular dose, lines) equals the receptor occupancy as a fraction of 1 and the intercept with the x-axis equals the $SUV_{0\text{-}60min}$ in the absence of specific binding (*4*). **B**) ○, Slopes of the Lassen plot in **A**. Solid line, fit with a saturation function, the minimum was fixed at 0 and receptor occupancy by the tracer was neglected. Fitted D_{50} (eliprodil dose at 50 % of fitted maximal occupancy) was 8.5 nmol/kg. Note that the Lassen plot assumes equal D_{50} and $SUV_{0\text{-}60min,min}$ for all brain regions and neglects occupancy by the tracer itself.

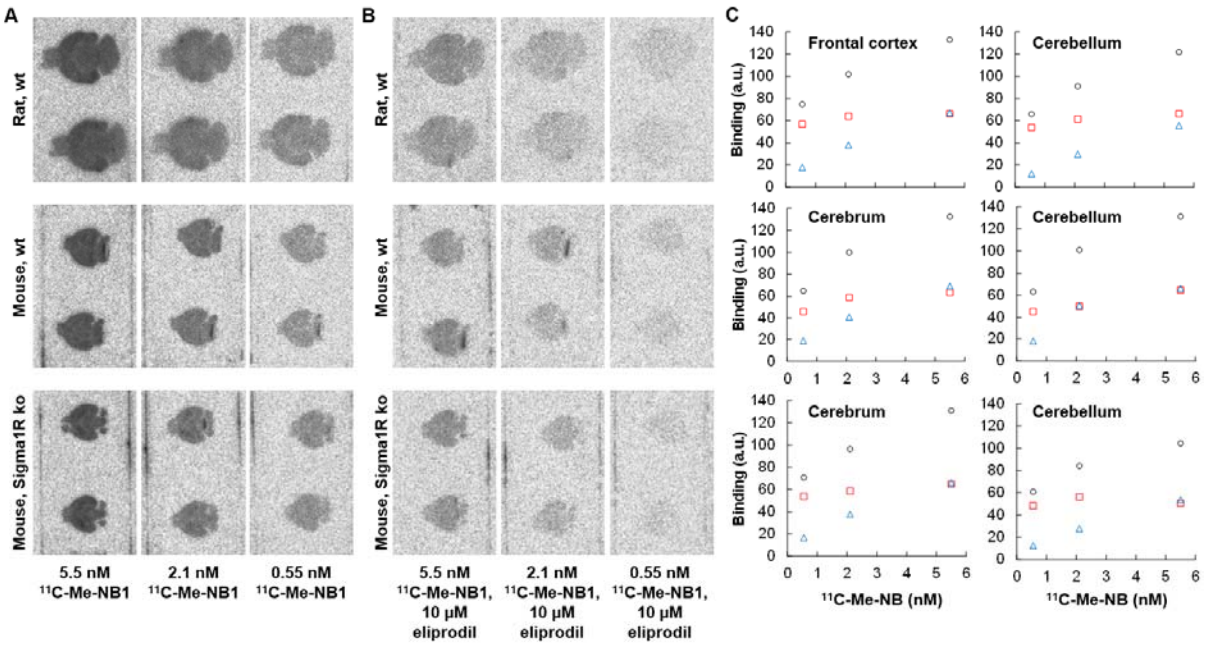

Supplemental Figure 14. *In vitro* autoradiography with brain slices from wt rats, wt mice and Sigma1R ko mice at 5.5 nM, 2.1 nM and 0.55 nM ^{11}C-Me-NB1 as indicated (**A**) and with 10 µM eliprodil for blocking (**B**). **C**) Bound radioactivity was quantified with PMOD v3.8 by region-of-interest analysis for cerebrum (mice), frontal cortex (rat) and cerebellum. The background-corrected radioactivity was averaged for the two brain slices per slide. Black circles, total bound radioactivity (as in **A**, background-corrected). Blue triangles, unspecific binding (as in **B**, background-corrected). Red squares, specifically bound tracer (difference between **A** and **B**). Note that specific binding is saturated already at the lowest investigated ^{11}C-Me-NB1 concentration of 0.55 nM, in agreement with the high affinity observed *in vivo* (**Fig. 2A** and **4A**). Note in addition the high specific binding in cerebellum of wt rat and mouse and of Sigma1R ko mouse, indicating off-target binding but excluding binding to Sigma1R.

Supplemental Tables

Supplemental Table 1 Binding affinities determined with rat brain membranes [a)]

Compound	Tritiated compound	Temperature (°C)	IC_{50} (nM) [b)]	K_i (nM) [c)]	n [d)]
Ro-25-6981	[^{3}H]ifenprodil	20	44.7 ± 11.0 [e)]	42.3 ± 12.0	3
	(+)-[^{3}H]pentazocine	20	23.1	15.4	1
Haloperidol	[^{3}H]ifenprodil	20	~ 8000		1
		37	~ 6000		1
	(+)-[^{3}H]pentazocine	20	753	482	1
		37 [f)]	38.0	31.9	1
Eliprodil	[^{3}H]ifenprodil	20	51.4 ± 33.9, 17-85	48.5 ± 32.0, 16-80	3
	(+)-[^{3}H]pentazocine	37	335-1281	229-875	3
Me-NB1	[^{3}H]ifenprodil	20	42.4 ± 2.9	40.2 ± 2.8	4
	(+)-[^{3}H]pentazocine	37	> 4000		3

[a)] Binding affinities were determined in a competition binding assay with rat brain membranes as described elsewhere (*5-7*) with 1 to 5 nM ^{3}H-ifenprodil or (+)-^{3}H-pentazocine (both PerkinElmer, Schwerzenbach, Switzerland). Ifenprodil binds with a K_d of 37 nM to the rat GluN1/GluN2B NTD binding site (*8*)) while (+)-pentazocine binds with a K_d 7 nM to rat Sigma1R (*9*). Sample volumes were 200 µL containing 0.1 mg (for assays with ^{3}H-ifenprodil) or 0.2 mg (assays with (+)-^{3}H-pentazocine) total protein in HEPES buffer (30 mM Na-HEPES, 110 mM NaCl, 5 mM KCl, 2.5 mM $CaCl_2$, 1.2 mM $MgCl_2$ at pH 7.4). Test compounds were added at various concentrations in triplicates and samples were incubated for 1 to 1.5 h at the indicated temperature or 2 to 2.5 h in the case of (+)-^{3}H-pentazocine at 37°C and filtered at 4°C as described elsewhere (*5*). The K_i values were calculated with the Cheng-Prusoff equation from the IC_{50} values determined in the binding assay and K_d of the tritiated compounds for the respective rat receptors, as indicated. [b)] Average ± standard deviation and/or range in case of 3 or more independent experiments, or results of individual experiments; [c)] Calculated with the Cheng-Prusoff equation and ifenprodil K_d =37 nM to rat brain NTD binding site (*8*) and (+)-pentazocine K_d=7 nM to rat Sigma1R (*9*), respectively; [d)] number of independent experiments with triplicates for each test concentration; [e)] similar results at 4°C (n=2) and 37°C (n=2); the mean K_i including all temperatures was 49.8 ± 19.7 nM. [f)] Inverse Sigma1R agonists such as haloperidol induce the formation of Sigma1R tetra- and oligomers, the suggested resting states of Sigma1R (*6*). The reduced form of haloperidol, formed by metabolism, irreversibly inhibits the receptor, in addition (*10*). Both would explain the temperature-dependent competition with (+)-^{3}H-pentazocine. Note that the bivalent cations in the HEPES buffer could affect the binding affinity (*1*).

Supplemental Table 2. Details of the PET scans with input function recording

Scan ID	Treat-ment [a)]	Body weight (g)	Injected dose (MBq)	Injected dose (nmol/kg)
1	V	320.6	31.83	0.44
3	V	352.8	36.47	0.59
5	V	319.1	51.66	0.78
7	V	341.1	33.68	0.47
Average ± SD	V	333.4 ± 16.4	38.41 ± 9.0	0.57 ± 0.15
2	K	328.4	33.16	0.69
4	K	310.7	40.69	0.54
6	K	341.4	38.5	0.46
Average ± SD	K	326.8 ± 15.4	37.5 ± 3.9	0.56 ± 0.12
Average ± SD	V,K	328.9 ± 17.5	39.8 ± 7.4	0.56 ± 0.14

[a)] V, vehicle; K, ketamine (25 mg/kg intraperitoneally, 30 min before tracer).

Supplemental Table 3. Fit composite parameters of the individual scans in Supplemental Table 2.

Scan ID	Treat-ment [a]	Model [b]	$V_{T,fit}$	$V_{T,Logan}$	BP_{ND}	V_S	V_{ND}	SUV (0-60min)	V_T of radio-metabolite	AICc [e]
1	V	2	12.57	12.54	2.67	9.14	3.43	2.94	0.19	266.1
		1	14.44		-	-	-	2.94	0.33	317.9
3	V	2	12.07	12.22	3.46	9.36	2.71	2.58	0.18	236.9
		1	11.87		-	-	-	2.58	0.14	332.7
5	V	2	10.71	10.68	3.19	8.15	2.56	2.41	0.17	250.4
		1	12.36		-	-	-	2.41	0.47	332.7
7 [c]	V	2	-	-	-	-		2.92		
		1			-	-		2.92		
Average ± SD [d]	V	2	11.78 ± 0.96	11.81 ± 0.99	3.11 ± 0.40	8.89 ± 0.64	2.90 ± 0.46	2.72 ± 0.26	0.18 ± 0.01	251.1 ± 14.6
Average ± SD	V	1	12.89 ± 1.37		-	-	-	2.72 ± 0.26	0.31 ± 0.16	327.7 ± 8.5
2 [c]	K	2			-	-	-	2.71		
		1			-	-	-	2.71		
4	K	2	12.34	12.45	5.04	10.30	2.04	2.62	0.05	244.8
		1	16.44		-	-	-	2.62	0.38	341.9
6	K	2	11.49	11.59	4.50	9.40	2.09	2.42	0.15	225.3
		1	14.26		-	-	-	2.42	0.48	379.3
Average ± SD	K	2	11.92	12.02	4.77	9.85	2.07	2.58 ± 0.15	0.10	235.1
Average ± SD	K	1	15.35		-	-	-	2.58 ± 0.15	0.43	360.6
Average ± SD	V,K	2	11.84 ± 0.75	11.90 ± 0.77	3.77 ± 0.97	9.27 ± 0.77	2.57 ± 0.56	2.59 ± 0.21	0.15 ± 0.06	244.7 ± 15.2
Average ± SD	V,K	1	13.87 ± 1.83		-	-	-	2.59 ± 0.21	0.36 ± 0.14	340.9 ± 23.1
Average ± SD	V,K	2 [f]	11.86 ± 0.69	11.75 ± 0.78	3.77 ± 1.01	9.29 ± 0.84	2.57 ± 0.55	2.59 ± 0.21	0	238.8 ± 18.3

[a] V, vehicle; K, ketamine (25 mg/kg intraperitoneally, 30 min before tracer). [b] 1, One-tissue compartment model; 2, two-tissue compartment model for parent tracer. One-tissue compartment model for radiometabolite in both cases. [c] No fit data available (see Methods). [d] SD, standard deviations shown for $n \geq 3$. [e] Corrected Akaike information criterion (Methods); residues are from brain TACs, residues of parent to total radioactivity in brain and plasma were not taken into account. [f] Distribution of the radiometabolite to the brain ignored.

Supplemental Table 4. Fit K_1, k_2, k_3 and k_4 of the individual scans of Supplemental Tables 2 and 3.

Scan ID	Treatment [a]	Model [b]	K_1 (mL/min/cm^3)	k_2 (1/min)	k_3 (1/min)	k_4 (1/min)
1	V	2	2.15	0.63	0.64	0.24
		1	1.70	0.12	-	-
3	V	2	2.42	0.89	0.63	0.18
		1	1.55	0.13	-	-
5	V	2	2.64	1.03	0.75	0.24
		1	1.71	0.14	-	-
7 [c]	V	2	-	-	-	-
		1	-	-	-	-
Average ± SD [d]	V	2	2.40 ± 0.25	0.85 ± 0.21	0.67 ± 0.07	0.22 ± 0.03
Average ± SD	V	1	1.66 ± 0.09	0.13 ± 0.01	-	-
2 [c]	K	2	-	-	-	-
		1	-	-	-	-
4	K	2	2.86	1.40	0.80	0.16
		1	1.64	0.10	-	-
6	K	2	4.38	2.09	0.83	0.19
		1	1.91	0.13	-	-
Average ± SD	K	2	3.62	1.75	0.81	0.17
Average ± SD	K	1	1.77	0.12	-	-
Average ± SD	V,K	2	2.89 ± 0.87	1.21 ± 0.57	0.73 ± 0.09	0.20 ± 0.04
Average ± SD	V,K	1	1.70 ± 0.13	0.12 ± 0.02	-	-
Average ± SD	V,K	2 [e]	2.91 ± 0.87	1.21 ± 0.56	0.74 ± 0.09	0.20 ± 0.04

[a] V, vehicle; K, ketamine (25 mg/kg intraperitoneally, 30 min before tracer). [b] 1, One-tissue compartment model; 2, two-tissue compartment model for parent tracer. One-tissue compartment model for radiometabolite in both cases. [c] No fit data available (see Methods). [d] SD, standard deviations shown for $n \geq 3$. [e] Distribution of the radiometabolite to the brain ignored.

References Supplemental Information

1. Mutel V, Buchy D, Klingelschmidt A, et al. In vitro binding properties in rat brain of [3H]Ro 25-6981, a potent and selective antagonist of NMDA receptors containing NR2B subunits. *J Neurochem.* 1998;70:2147-2155.

2. Krämer SD. Positron Emission Tomography (PET): Quantification and Kinetic Modeling. *Reference Module in Chemistry, Molecular Sciences and Chemical Engineering*. Amsterdam (NL): Elsevier; 2015.

3. Logan J, Fowler JS, Volkow ND, et al. Graphical analysis of reversible radioligand binding from time-activity measurements applied to [N-11C-methyl]-(-)-cocaine PET studies in human subjects. *J Cereb Blood Flow Metab.* 1990;10:740-747.

4. Cunningham VJ, Rabiner EA, Slifstein M, Laruelle M, Gunn RN. Measuring drug occupancy in the absence of a reference region: the Lassen plot re-visited. *J Cereb Blood Flow Metab.* 2010;30:46-50.

5. Milicevic Sephton S, Mu L, Schweizer WB, Schibli R, Krämer SD, Ametamey SM. Synthesis and evaluation of novel alpha-fluorinated (E)-3-((6-methylpyridin-2-yl)ethynyl)cyclohex-2-enone-O-methyl oxime (ABP688) derivatives as metabotropic glutamate receptor subtype 5 PET radiotracers. *J Med Chem.* 2012;55:7154-7162.

6. Chu UB, Ruoho AE. Sigma receptor binding assays. *Curr Protoc Pharmacol.* 2015;71:1 34 31-21.

7. Nguyen VH, Kassiou M, Johnston GA, Christie MJ. Comparison of binding parameters of sigma 1 and sigma 2 binding sites in rat and guinea pig brain membranes: novel subtype-selective trishomocubanes. *Eur J Pharmacol.* 1996;311:233-240.

8. Schoemaker H, Allen J, Langer SZ. Binding of [3H]ifenprodil, a novel NMDA antagonist, to a polyamine-sensitive site in the rat cerebral cortex. *Eur J Pharmacol.* 1990;176:249-250.

9. Cagnotto A, Bastone A, Mennini T. [3H](+)-pentazocine binding to rat brain sigma 1 receptors. *Eur J Pharmacol.* 1994;266:131-138.

10. Cobos EJ, del Pozo E, Baeyens JM. Irreversible blockade of sigma-1 receptors by haloperidol and its metabolites in guinea pig brain and SH-SY5Y human neuroblastoma cells. *J Neurochem.* 2007;102:812-825.